# Measured densities and derived thermodynamic properties of CO2-rich mixtures in gas, liquid and supercritical phases from 273 K to 423 K and pressures up to 126 MPa

# Measured densities and derived thermodynamic properties of $CO_2$-rich mixtures in gas, liquid and supercritical phases from 273 K to 423 K and pressures up to 126 MPa

Mahmoud Nazeri[a*], Antonin Chapoy[a*], Rod Burgass[a], Bahman Tohidi[a]

[a] *Hydrates, Flow Assurance & Phase Equilibria Research Group, Institute of Petroleum Engineering, Heriot-Watt University, Edinburgh, EH14 4AS, UK*

** Corresponding Authors: Mahmoud Nazeri (M.Nazeri@hw.ac.uk)*

*Antonin Chapoy (A.Chapoy@hw.ac.uk)*

## ABSTRACT

The densities of three multi-component mixtures with high $CO_2$ content and common impurities, i.e. hydrocarbons, nitrogen, hydrogen, oxygen, argon and carbon monoxide, were measured using an Anton Paar DMA-HPM densitometer. The mixtures include MIX 1 with 0.9564 mole fraction $CO_2$ and 0.0436 mole fraction impurities of methane and non-condensable gases, MIX 2 with 0.8983 mole fraction $CO_2$ and 0.1017 mole fraction impurity of non-condensable gases and MIX 3 with 0.6999 mole fraction of $CO_2$ and 0.3001 mole fraction of light hydrocarbons. First, the densitometer was calibrated using pure $CO_2$ and then the density measurements of mixtures were carried out in the gas, liquid and supercritical phases at pressures up to 126 MPa at various isotherms of $T$/K = 273, 283, 298, 323, 373 and 423. The obtained data then were employed to evaluate the classical cubic equations of state (SRK and PR). In addition, the $CO_2$ volume correction term and the Peneloux shift parameter were introduced to improve density predictions. Comparisons show that applying $CO_2$ volume correction term to SRK EoS with modified $k_{ij}$ could improve the density predictions and the AAD was reduced from 4.7% to 1.9%. In addition to the classical cubic equations of state, the new measured data were used to evaluate the GERG EoS. The AAD of the GERG EoS from experimental data measured in this work are 2.8%, 1.0% and 1.2% in the gas, liquid and supercritical phases, respectively. The overall AAD of GERG EoS from the new density data in this work is 1.7%. Thermodynamic properties, i.e. compressibility factor, specific heat capacity, speed of sound and Joule-Thomson coefficient, were then calculated from the

experimental density data using thermodynamic equations. Following this the derived properties were compared to the predictions made with the GERG equation of state.

*Keywords: Density measurement, high pressure, Carbon capture transport and storage (CCS), $CO_2$ and impurities, Thermodynamic properties, effect of impurities*

## 1. Introduction

The application of carbon capture and storage (CCS) has become increasingly important, from both scientific and industrial points of view, the overall aim being to reduce $CO_2$ emissions. CCS is a promising technology-based solution to reduce the significant amount of $CO_2$ release from large-scale industrial sources. In the CCS full chain, the $CO_2$ emissions from the industry sector need to be captured with emerging technologies such as pre-combustion, post-combustion and oxyfuel processes. The captured $CO_2$ then can be transported either by pipelines or ships to storage locations such as depleted oil and gas reservoirs, saline aquifers or unmineable coal seams [1]. Transport by pipeline is the preferred option for the large quantities of carbon dioxide over longer distances [2]. Technically, $CO_2$ can be transported through pipelines in the form of a gas, a supercritical fluid or in the sub-cooled liquid state. Operationally, the most efficient $CO_2$ pipelines used for enhanced oil recovery transport the $CO_2$ as a supercritical fluid [3]. As the critical point of $CO_2$ ($P_c$ = 7.38 MPa and $T_c$ = 304.3 K) and triple point ($P_t$ = 0.518 MPa at $T_t$ = 216.6 K) are very different from conventional fluids present in transport pipelines in oil and gas industry, the modeling of these pipelines poses new challenges [4]. It was proposed that the operating pressure of $CO_2$ transport pipelines should be above 8.6 MPa to make sure that the fluid will always be in the single super critical phase over a range of temperatures that the pipeline may encounter [5]. The captured $CO_2$ in the first step may contain various types and levels of impurities depending on the source and capturing technology [6][7][8]. The presence of impurities, particularly hydrogen and nitrogen, can change the fluids thermophysical properties such as critical pressure, density and viscosity, which could compromise the performance of the CCS processes. In the design of $CO_2$ transport pipeline, the overestimation or underestimation of the fluid physical properties, particularly the density of $CO_2$ mixtures with impurities, may results in the underdesign or overdesign of the pipeline diameter. This can cause operational problems such as high velocity and erosion or phase change and causing multiphase flow in the pipeline [9][10][11]. $CO_2$ and $CO_2$-rich

mixtures also play an important role in $CO_2$ enhanced oil recovery. The $CO_2$-rich mixtures may cause hydrate formation problem during the transportation [12][13].

Equations of state (EoS) are imperative to predict and understand the thermodynamic properties of fluids. Several equations of state are available in literature to predict the properties of high $CO_2$ content mixtures [14][15][16][17]. In this work, new measured density data are presented for three multi component $CO_2$-rich mixtures. The classical cubic equations of state Soave-Redlich-Kwong (SRK-EoS) [18] and Peng-Robinson (PR-EoS) [19] with $CO_2$ volume correction [20][21] (SRK-$CO_2$ and PR-$CO_2$) and Peneloux shift parameter [22] (SRK-Pen and PR-Pen) as well as the GERG EoS then were evaluated using the measured density data. The thermodynamic properties, i.e. compressibility factor, specific heat capacity, speed of sound and joule-Thomson coefficient also were calculated from the measured density data and were compared with the GERG EoS [23].

## 2. Literature review

According to the requirements of engineering applications for design and operation of $CO_2$ capture and storage systems, cubic equation of states are preferable to predict VLE properties and density calculations [16] due to the simplicity and availability in the oil and gas industry as well as commercial software packages. The systems to be studied may contain a wide range of components including pure $CO_2$, and mixtures with other gases, amines, ionic liquids, water, and brines. Some studies were conducted to investigate thermodynamic properties of $CO_2$ and $CO_2$-mixture systems using equations of state.

The SRK EoS was investigated by Frey et al. [24] for density and phase equilibria of mixtures, including the $CO_2$-$H_2O$ and $CO_2$-$CH_4$ binary systems. They applied a density and temperature dependent volume translation function on SRK EoS. They found that selection of mixing rules has a significant influence on the results of their method, which is abbreviated as DMT. Also, Thiery et al. [25] evaluated the SRK EoS for VLE and volume calculations of $CO_2$-$N_2$, $CO_2$-$CH_4$ and $CO_2$-$CH_4$-$N_2$. Their results showed that with the SRK EoS, the average deviation for the saturated pressures is around 1% in the temperature range of 208.45-270 K for the $CO_2$-$CH_4$ system, 4% in the temperature range of 218.15-273.15 K for the $CO_2$-$N_2$ system, and 2-3% for the $CO_2$-$CH_4$-$N_2$ system.

The PR and Patel-Teja (PT) EoS were investigated by Al-Sahhaf et al. [26] for VLE of the $N_2$-$CO_2$-$CH_4$ ternary system. Also, Boyle and Carroll [27] investigated PR, SRK, PT, PR-Peneloux, SRK-Peneloux and PR-Mathias EoS for density calculations of $CO_2$-$H_2S$. The results showed that PT is the most accurate EoS in liquid region, supercritical region, and

overall, with an AAD of 2.16%, 2.26% and 1.82% respectively; while SRK is the most accurate EoS in the vapor region with an AAD of 0.51%. Seven cubic equations of state were evaluated with respect to VLE and density of $CO_2$ mixtures including $CH_4$, $N_2$, $O_2$, $H_2S$, $SO_2$ and Ar using many of the experimental data presented by Li et al. [16] [28][29]. The EoS evaluated were PR, RK, SRK, PT, PR-Peneloux, SRK-Peneloux and the improved SRK. The binary interaction parameters, $k_{ij}$, were calibrated with respect to VLE data.

Mantovani et al. [30] presented experimental data for supercritical $CO_2$ binary systems of nitrogen, oxygen and argon used in oxy-fuel capture process with almost 5% and 10% impurities. They used vibrating tube densitometer for pressures ranging from 1 MPa to 20 MPa at different temperatures from 303 to 383 K. They also tuned the binary interaction parameters against experimental data using PR, SRK-Peneloux and Benedict-Webb-Rubin-Starling (BWRS) equations of state. For the $CO_2$-$N_2$ systems, they reported an AAD of 2.10%, 3.05% and 1.71% for PR, SRKP and BWRS, respectively. Also, the AAD of 2.37%, 3.92% and 1.97% for those of $CO_2$-$O_2$ systems and 2.56%, 4.07% and 1.75% for those of $CO_2$-Ar systems. All the AADs reported using the new regressed $k_{ij}$ parameters. It can be seen that for each case, BWRS can predicts better than cubic equation of states. Sanchez-Vicente et al. [31] presented the density data for three $CO_2$-$H_2$ mixtures, as the main impurity of pre-combustion capturing process, with 2%, 7.5% and 10% of hydrogen at 288.15–333.15 K and pressures between 1.5 and 23 MPa. They then compared their density data with the values calculated by the GERG-2004 equation of state using the original parameters provided by Kunz et al. [15]. The deviations between the experimental and calculated density are also calculated and analyzed in the critical and liquid regions of the mixtures. They have concluded that 2% hydrogen can reduce the molar density of $CO_2$ up to 25% in the critical region which can significantly affect the compression and transportation development for CCS. They also have found that the GERG-2004 EoS can accurately predict the density of $CO_2$-rich systems with low $H_2$ concentration (2%) with an AAD of 0.6% while for the high $H_2$ concentrations, AADs of up to 4% and 14% were observed for the liquid phase and supercritical phase, respectively.

Rivas et al. [32] measured density of $CO_2$-$CH_4$ and $CO_2$-CO systems at $T$/K = 304.21 and 308.14 and pressures ranging from 0.1 to 20 MPa and $x_{CO2}$ (mole fraction of carbon dioxide in vapor phase) > 0.97. Then, they compared the volumetric behavior of these systems to the PR, PC-SAFT and GERG equations of state. The deviations were reported less than 3.5% for PR, 2.8% for rescaled PC-SAFT and 1.0% for GERG. The VLE experimental data for various binary systems containing $CO_2$ were measured at various temperature and pressures for $CO_2$ - Ar [33], $CO_2$ - $H_2$ [34], $CO_2$ - $N_2$ [34][35]and $CO_2$ - $O_2$ [36]. The density of 0.95 $CO_2$ – 0.05

Ar was measured by Yang et al. [37] in the vapor phase at pressures up to 9.0 MPa. The experimental data also were evaluated by GERG-2008 and EOS-CG equations of state with the relative deviation of 0.95% and 0.18%, respectively. The densities of 0.95 $CO_2$ – 0.05 $H_2S$ also was measure by Nazeri et al. [21] at pressures up to 42 MPa and various isotherms in the gas, liquid and supercritical phases. The densities of two ternary systems of Ar-$N_2$-$CO_2$ with different concentrations were measured by Yang et al. [38] at pressures from 3 to 31 MPa at temperatures from 323 to 423 K in supercritical phase. The deviation of GERG-2008 from experimental data was reported to be 0.6%.

## 3. Experimental

### *3.1 Material*

Varieties of multi-component mixtures with diverse impurities and different percentages were prepared, as shown on Table 1. Each mixture represents the composition of gas from a specific source. MIX 1 with 0.0436 mole fraction of impurities such as methane, nitrogen, hydrogen, argon, oxygen and carbon monoxide can show a proper behavior of the streams suitable for the carbon capture, transport and storage. MIX 2 with a wider range of 0.1017 mole fraction of non-condensable gases, i.e., nitrogen, oxygen and argon, was also prepared to mimic the CCS stream fluids. Mixture 3 with 0.3001 mole fraction of light hydrocarbons and 0.6999 mole fraction $CO_2$ represents the composition of a gas field in South East Asia. The mixtures supplied by BOC were certified on the basis of gravimetry in accordance with ISO 6142 with analytical validation. The volume of the cylinders were about 2 cubic meters. It is recommended by the supplier not to use the product below 5% of actual contents. According to the suppliers' instructions to prevent condensation, the cylinders were kept in the laboratory area with a temperature of about 293.15 K (20 °C). The reported expanded uncertainties in each table are based on a standard uncertainty multiplied by a coverage factor $k = 2$, providing a level of confidence of approximately 95%.

### *3.2 Equipment description*

The densities of $CO_2$-rich systems were measured using a high temperature and pressure oscillating U-tube densitometer, Anton Paar DMA-HPM, which consists of a measuring cell and an evaluation unit. A schematic view of the apparatus is shown in Figure 1. The equipment was described in the previous publication [20]. Briefly, the measuring cell includes a U-shaped Hastelloy C-276 tube that is excited to vibrate at its characteristic frequency electronically. The

DMA-HPM is connected to an mPDS 2000V3 evaluation unit which measures the oscillation period. The resolution of the unit is seven significant digits.

The temperature of the densitometer is controlled by an oven, manufactured by BINDER GmbH, which can be used at temperatures between −70 °C to 200 °C (203 - 473 K). The measuring U-shaped cell is insulated from the environment keeping the temperature stable to ±0.02 K. A built-in thermometer which is connected to the mPDS 2000V3 unit shows the temperature of the vibrating tube cell. A hand pump which can inject or withdraw the mercury to the set-up is used to control the system pressure. Two Quartzdyne pressure transducer (model: QS 30K-B) with the design pressure up to 207 MPa and standard uncertainty of ±0.02 MPa [39] were connected to record the system pressure.

### *3.3 Measurement and calibration procedure*

All the experiments were conducted using the Anton Paar densitometer. In each test, after applying vacuum to the entire system, the sample was injected through the injection point on top of the densitometer. It should be pointed out that the sample fluid during the injection was kept in single phase to avoid composition change due to flashing. Then after disconnecting the sample cylinder from the system, it was allowed to stabilize at the desired temperature. When the temperature of the vibrating tube was stable, the desired pressure was set using the hand pump. Once conditions had stabilized, the oscillation period of the U-tube was determined from the interface mPDS 2000V3 evaluation unit.

The measurement of density with a vibrating tube densitometer is not absolute, thus, the raw data (period of oscillation) should be further treated to obtain the densities. The relationship between them is:

$$\rho(\mathrm{T},\mathrm{P}) = \mathrm{A}(\mathrm{T},\mathrm{P})\tau^2(\mathrm{T},\mathrm{P}) - \mathrm{B}(\mathrm{T},\mathrm{P}) \tag{1}$$

where $\rho(T,P)$ is the sample density at temperature $T$ and pressure $P$, $\tau(T,P)$ is the period of oscillation at temperature and pressure, $A(T,P)$ and $B(T,P)$ are the apparatus parameters depending on temperature and pressure, and they must be determined from calibration measurements. For calibration, $CO_2$ density can be used as a reference substance at two different pressures (the lowest and the highest desired pressures in the system at the same temperature) in gas, liquid and supercritical phases. The apparatus parameters then were defined as follows:

$$\mathrm{A}(\mathrm{T},\mathrm{P}) = \frac{\rho(\mathrm{T},\mathrm{P}_1) - \rho(\mathrm{T},\mathrm{P}_2)}{\tau^2(\mathrm{T},\mathrm{P}_1) - \tau^2(\mathrm{T},\mathrm{P}_2)} \tag{2}$$

$$B(T,P) = \frac{\tau^2(T,P_2)\rho(T,P_1) - \tau^2(T,P_1)\rho(T,P_2)}{\tau^2(T,P_1) - \tau^2(T,P_2)} \quad (3)$$

During our calibration, the densities of pure $CO_2$ were measured at different desired pressures for each isotherm. The density data used for calibration were calculated with the Span and Wagner multi-parameter equation of state [40]. Then, the parameters *A* and *B* were calculated by plotting the linear trend line for density versus squared oscillation period measured at different desired pressures at each isotherm. The procedure was repeated for each isotherm once at low pressures, i.e. gas phase, then at higher pressures, i.e. dense liquid / supercritical phases. Figure 2 and Figure 3 show the procedure to determine *A* and *B* parameters at 373.15 K (100 ºC) at low and high pressures, respectively. All calibration data for each isotherm at low pressures (gas phase) and high pressures (dense phase) can be seen in Table 2 and Table 3, respectively. Finally, the *A* and *B* calibration parameters at low and high pressures at different measuring temperatures can be found in Table 4.

### *3.4 Density validation*

The measured densities for pure $CO_2$ and MIX 1 were compared to the density data measured by Al-Siyabi et al. [41]. As shown on Figure 4, the deviations of the experimental data measured in this work from the PR-$CO_2$ EoS using pure $CO_2$ were compared to the deviations of the Al-Siyabi et al work at various isotherms. The densities measured by Al-Siyabi et al. are only in the dense liquid / supercritical phase while in this work, the densities were measured in both gas and dense phases. Also, the deviations of the measured density of multi component mixture, MIX 1, from the PR-$CO_2$ equation of state can be seen at two isotherms 283.15 K and 323.15 K in Figure 5. The comparisons demonstrate that the density measurements are in good agreement with experimental data in literature as well as with prediction by equation of state.

### *3.5 Density measurement uncertainties*

The combined standard uncertainties [42] of density measurements for each measured quantity were calculated using the root sum of the squares of uncertainties as shown in the following equation.

$$u_c(\rho) = \sqrt{u_1(T)^2 + u_2(p)^2 + u_3(\tau)^2 + u_4(x)^2} \quad (4)$$

where, $u_1(T)$ is the estimated uncertainties due to the temperature, $u_2(p)$ the estimated uncertainties due to pressure, $u_3(\tau)$ the estimated uncertainties of oscillation period and $u_4(\tau)$ the estimated uncertainties of the composition.

The estimated uncertainties due to temperature variations, $u_1(T)$, was calculated from the equation below:

$$u_1(T) = \sqrt{\left(\frac{\partial \rho}{\partial T}\right)^2 . u(T)^2} \quad (5)$$

In the above equation, *u(T)* is the standard estimated uncertainty of temperature probe and is considered to be 0.02 K [43]. The density gradient due to the temperature variations, $\left(\frac{\partial \rho}{\partial T}\right)$, was calculated from the equation below.

$$\left(\frac{\partial \rho}{\partial T}\right) = \frac{1}{2u(T)}\left(\rho_{T+u(T)} - \rho_{T-u(T)}\right) \quad (6)$$

The upper and lower limits of densities due to temperature effect, $\rho_{T+u(T)}$ *and* $\rho_{T-u(T)}$, were estimated from REFPROP *v8.0* [40]. A similar procedure was followed to estimate the uncertainties due to the pressure and period of oscillation. The standard uncertainty of high pressure Quartzdyne pressure transducer (model: QS 30K-B), *u(p)*, is determined 0.02 MPa [39] and standard uncertainty of oscillation period, *u(τ)*, is 0.005 μs [44].

$$u_2(p) = \sqrt{\left(\frac{\partial \rho}{\partial p}\right)^2 . u(p)^2} \quad (7)$$

$$\left(\frac{\partial \rho}{\partial p}\right) = \frac{1}{2u(p)}\left(\rho_{T+u(p)} - \rho_{T-u(p)}\right) \quad (8)$$

$$u_3(\tau) = \sqrt{\left(\frac{\partial \rho}{\partial \tau}\right)^2 . u(\tau)^2} \quad (9)$$

$$\left(\frac{\partial \rho}{\partial \tau}\right) = \frac{1}{2u(\tau)}\left(\rho_{T+u(\tau)} - \rho_{T-u(\tau)}\right) \quad (10)$$

$$u_4(\tau) = \sqrt{\left(\frac{\partial \rho}{\partial x}\right)^2 . u(x)^2} \quad (11)$$

$$\left(\frac{\partial \rho}{\partial x}\right) = \frac{1}{2u(x)}\left(\rho_{T+u(x)} - \rho_{T-u(x)}\right) \quad (12)$$

Finally, the expanded uncertainty of each measured density, *U(ρ)*, were calculated by multiplying to coverage factor, *k*. In this work, the coverage factor *k = 2* was used to give a level of confidence of 95% for uncertainty of measurements.

$$U(\rho) = k\, u_c(\rho) \quad (13)$$

## 4. Modeling

The measured densities were used to evaluate the density predictions using classical cubic equations of state. In this work, SRK [18] and PR [19] equations of state were used to predict the densities. The modified binary interaction parameters, $k_{ij}$, shown in Table 5 and Table 6 for

PR [19] and SRK [18] equations of state, were employed to improve the phase equilibrium predictions. To improve the density predictions, also the $CO_2$ volume correction term [20][21] and Peneloux volume translation parameter [22] were applied to the SRK [18] and PR [19] equations of state.

Compressibility factors of the investigated mixtures were obtained from the real gas law, i.e. $Z=p/\rho RT$. Other thermodynamic properties such as isobaric heat capacity, speed of sound and Joule-Thomson coefficient were calculated from the Soave modifications [45][46] on the Benedict–Webb–Rubin (BWR) equation of state [47] by simplifying the original BWR equation as below:

$$Z = \frac{p}{\rho RT} = 1 + B\rho + D\rho^4 + E\rho^2(1 + F\rho^2)\exp(-F\rho^2) \qquad (14)$$

In this work, the parameters *B, D, E* and *F* were optimized using the measured density data. The derived thermodynamic properties then were calculated [48] and compared to the GERG EoS [23]. The calculation procedure from the thermodynamic equations was explained in detail in the previous publication [48].

## 5. Results and discussions

First, the densitometer was calibrated using pure $CO_2$ at lower pressure conditions, i.e. in the gas phase and at elevated pressures, i.e. in the liquid and supercritical phases for each isotherms. Then, densities of three multi-component mixtures, MIX 1 with 0.0436 mole fraction impurity, MIX 2 with 0.1017 mole fraction impurity and MIX 3 with 0.3001 mole fraction impurity were measured at pressures ranging from 1 to 126 MPa at six different isotherms, *T*/K = 273.15, 283.15, 298.15, 323.15, 373.15 and 423.15 in the gas, liquid and supercritical regions. Both experimental results and modeling predictions using PR and SRK EoSs, those with the $CO_2$ correction volume and Peneloux shift parameter, as well as the GERG EoS, are shown in Table 7 through Table 9 and Figure 6 through Figure 13. In each table, the measured densities as well as the estimated uncertainties of measurements are shown at the corresponding pressure, temperature and phase. Also, the calculated density using PR EoS, that with $CO_2$ correction volume, with Peneloux shift parameter and the GERG EoS are presented in the tables. Finally, corresponding relative deviations of the models from experimental density for each measurement are also shown in each table. In addition, the Absolute Average Deviations (AADs) for all data are listed in the tables.

### *5.1. Measurement uncertainties*

Table 10 shows the average and maximum estimated expanded uncertainties of density measurements in this work. The expanded uncertainties were reported with a level of confidence of 95% by multiplying the calculated combined standard uncertainty, $u_c(\rho)$, by coverage factor of $k = 2$ [42]. The average expanded uncertainties, $U(\rho)$, in the gas phase is 1.9% while in the dense liquid / supercritical phases is 0.4%. The maximum expanded uncertainty in the gas phase were reported 4.5% for MIX 1 at very low pressure and temperature while that in the dense liquid and supercritical phases is 0.9% and 1.3%, respectively. Generally, the uncertainties of measurements are higher at very low pressures in the gas phase as well as at points closed to the two-phase region in either the gas or liquid phase.

### *5.2. Evaluations of models*

Table 11 summarizes the AAD and Maximum Absolute Deviation (MAD) of the models with PR and SRK equations of state using $CO_2$ volume correction, original and Peneloux shift parameters, from experimental data for each material at different regions. As can be seen, SRK-$CO_2$ equation of state predicts slightly more accurately compared to the PR-$CO_2$ EoS. The overall AADs for SRK and PR using $CO_2$ volume correction are 1.9% and 2.2%, respectively. The prediction accuracy of SRK-$CO_2$ in the gas, liquid and supercritical phases are higher than the PR-$CO_2$. The AAD for SRK-$CO_2$ in those phases are 2.9%, 1.6% and 1.3%, respectively. While those for the PR-$CO_2$ are 3.1%, 1.7% and 1.7%, respectively. The predictions of SRK and PR with modified $k_{ij}$ without density correction parameters are almost in the same accuracy with the overall AAD of 4.7% and 4.8%, respectively. In the gas phase, the accuracy of SRK with the AAD of 2.8% is higher than PR with the AAD of 3.4%, while in the dense liquid / supercritical phase, the predictions of PR (AADs of 5.5% / 5.4%) is relatively better than the SRK (AADs of 5.8% / 5.7%). Using the Peneloux shift parameters to predict the density of $CO_2$ systems can result in an overall AAD of 3.0% and 4.1% for PR-Pen and SRK-Pen, respectively. The AADs in the gas phase are 2.8% and 3.2%, in the liquid phase are 4.5% and 2.6% and in the supercritical phase are 5.0% and 3.1% for SRK-Pen and PR-Pen, respectively.

By comparing the AADs of classical cubic equations of state, it is clear that $CO_2$ volume correction with PR and SRK equations of state can predict well compared to those without density correction term or those using Peneloux shift parameters for $CO_2$-rich mixtures. In the gas phase, SRK and SRK-Pen are the best models to predict the density with the AAD of 2.8%,

while in the dense liquid / supercritical phases, the SRK-$CO_2$ is the most accurate with the AADs of 1.6% / 1.3%. Overall, the SRK-$CO_2$ is the most accurate model to predict the density with the AAD of 1.9%.

The GERG multi parameter EoS was also evaluated by comparing predictions to the new experimental data measured in this work. As shown on Table 11, the AAD of the GERG EoS in the gas, liquid and supercritical phases are 2.8%, 1.0% and 1.2%, respectively. The overall AAD of GERG EoS is also 1.7%. This means GERG EoS predicts the densities of investigated mixtures more accurately than the classical cubic EoSs which SRK-$CO_2$ with the AAD of 1.9% was the most accurate EoS.

### *5.3. Effect of impurities on the density reduction of pure $CO_2$*

Increasing the density of $CO_2$ fluids will reduce the pipeline size and the running cost. However, the presence of common impurities in $CO_2$ stream will reduce the density of pure $CO_2$. The amount of reduction is a function of the mixture composition and pipeline operating pressure and temperature. The lighter components tend to reduce the density more. Also, the amount of reduction could be high at pressures and temperatures close to the critical pressure and temperature of the mixture. In order to investigate this effect, spline interpolation is implemented to the modeling and experimental data. Table 12 and Figure 12 to Figure 14 show the reduction in $CO_2$ density for tests conducted at 323 K (50 °C). A maximum reduction of the $CO_2$ density at a certain pressure for a given temperature is observed for the $CO_2$ mixtures. The maximum reduction is 21.7% in MIX 1 ($MW$ = 43.64), 33.9% in MIX 2 ($MW$ = 42.75) and 38.5% in MIX 3 ($MW$ = 37.60). The maximum reduction occurs at pressure around 11 MPa for MIX 1 and MIX 2 and at 12.4 MPa for MIX 3.

### *5.4. Derived thermodynamic properties*

Thermodynamic properties were obtained from the measured density data. Table 13 summarizes the AADs of the calculated properties from the GERG EoS [23] for all mixtures. Figure 15 and Figure 16 show the compressibility factor of MIX 1 versus density at various measured isotherms at total pressure ranges and lower pressure ranges, respectively. The obtained data then were compared to the prediction results using GERG EoS. Figure 17 shows the relative deviations the GERG predictions from the calculated compressibility factor at different isotherms, while Figure 18 shows the deviations for all three investigated mixtures. As can be seen, the predictions are in good agreement with the calculated data. The AADs of

GERG predictions from calculated compressibility factor for the investigated mixtures are 2.9% and 1.0% / 1.3% for the gas and dense liquid / supercritical phases with the overall AAD of 1.7%.

The derived specific heat capacities from the measured density data at various isotherms for the MIX 1 are shown in Figure 19. The lines in the figure show the predictions using GERG EoS which is in good agreement with the experimentally calculated specific heat capacities. Figure 20 shows the deviations of investigated mixtures from the GERG EoS. The overall AADs for MIX 1 to MIX 3 are 0.8%, 7.5% and 3.5%, respectively. The AAD for the investigated mixtures in the gas phase is 2.1%, while that of dense liquid / supercritical phases is 3.4% / 5.0%, respectively. The overall AAD of GERG predictions for the specific heat capacity of investigated mixtures is 3.5%.

Figure 21 illustrates the calculated speed of sound as well as the predictions using GERG EoS for the mixture 1 at various isotherms. As can be seen, GERG EoS can predicts the speed of sound accurately. The AADs for the mixture 1 in the gas, liquid and supercritical phases are 0.9%, 4.4% and 1.0% with the overall AAD of 2.1%, respectively. Figure 22 also demonstrates the deviations of the calculated speed of sound for the three studied mixtures from the GERG EoS predictions. As can be seen in Table 13, the AADs of speed of sound for the studied mixtures in the gas, liquid and supercritical phases are 0.5%, 6.8% and 2.6% with the overall AAD of 3.1%, respectively.

The Joule-Thomson coefficients, $\mu_{JT}$, of MIX 1 at measured temperatures are shown in Figure 23. The lines are predictions using GERG EoS, while the points show the calculated data from the measured densities. Figure 24 shows the deviations of GERG predictions from the calculated data for all investigated mixtures. As can be seen in this figure, the $\mu_{JT}$ can reach the deviations about -50% for MIX 2 at 273 and 283 K in the area in the vicinity of bubble curve. The AAD of GERG from the calculated Joule-Thomson coefficient in the gas, liquid and supercritical phases are 5.2%, 10.3% and 10.0% with the overall AAD of 8.4%, respectively.

## 6. Conclusions

Undoubtedly, thermodynamic properties of $CO_2$ mixtures play an important role in the design and modeling of CCS infrastructures. This work was concentrated on the density measurement and modeling of various multi component mixtures. The densities of the mixtures were measured in the gas, liquid and supercritical regions after calibrations using pure $CO_2$ at each desired isotherm. It was concluded that the uncertainty of measurements in the gas phase is much higher than dense liquid / supercritical phases. The standard uncertainty of the pressure

transducer at lower pressures can result in higher uncertainty of the measured density in the gas phase. Also, it is obvious that the uncertainties of the measurement at few points which are in the vicinity of two-phase region are high due to the sharp changes of densities with pressure changes.

The importance of equations of state to predict the thermodynamic properties, particularly density, is evident. In the density modeling part of this work, two cubic equations of state, SRK and PR, as well as the GERG EoS were studied. These two classical cubic equations were selected due to the popularity in the oil and gas industry and availability in commercial software packages. Also, $CO_2$ volume correction was introduced to these cubic EoSs to improve the density prediction in the dense phase. It is concluded that generally both SRK and PR with $CO_2$ volume correction have acceptable predictions with AAD of 1.9% and 2.2%, respectively. The predictions by SRK in the gas phase are slightly more accurate than PR, while in the dense liquid / supercritical phase, predictions by PR are better than SRK. It also was concluded that introducing the $CO_2$ volume correction to the original equations improves the density predictions significantly in the dense liquid / supercritical phases. Overall, the AAD for PR was reduced from 4.8% to 2.2% by introducing the $CO_2$ volume correction. Those for SRK were reduced from 4.7% to 1.9%. The other conclusion worth noting is that the accuracy of predictions using $CO_2$ volume correction is higher than that using Peneloux shift parameter. It was also concluded that the GERG EoS is able to predict the densities of investigated mixture more accurately compared to the classical cubic EoSs. The overall AAD of GERG from the new measured data is 1.7%.

Moreover, the reduction in density of pure $CO_2$ due to the presence of impurities in the supercritical phase also was investigated for each mixture. It was concluded that a maximum reduction of the pure $CO_2$ density at a given temperature of 323.15 K (50 °C) was observed at pressures approximately 11 to 12 MPa depends on the composition of mixtures. Overall, lighter molecular weight impurities tend to reduce $CO_2$ density much more than those with a molecular weight close to pure $CO_2$.

Thermodynamic properties were also obtained from the measured density data. The calculated data then were used to evaluate the GERG EoS. The AADs of 1.7%, 3.5%, 3.8%, 3.1% and 8.4% were achieved for the *Z*-factor, isobaric and isochoric heat capacities, speed of sound and Joule-Thomson coefficient, respectively.

**Acknowledgements**

The JIP project" Impact of Common Impurities on Carbon Dioxide Capture, Transport and Storage" [20] was conducted jointly at Heriot-Watt University in UK and MINES ParisTech in France from 2011 - 2014. Thermophysical properties measured during the course of project were phase equilibira, hydrates [12], solid formation, density [21][49], viscosity, interfacial tension [50], solubility [51][52][53] and pH. This project was sponsored by Chevron, GALP Energia, Linde AG Engineering Division, OMV, Petroleum Expert, Statoil, TOTAL and National Grid Carbon Ltd, which is gratefully acknowledged.

## REFERENCES


[1] *IPCC, 2005: IPCC special report on carbon dioxide capture and storage. Prepared by Working Group III of the Intergovernmental Panel on Climate Change [Metz, B., O. Davidson, H. C. de Coninck, M. Loos, and L. A. Meyer (eds.)]*. Cambridge University Press, Cambridge, United Kingdom and New York, NY, USA.

[2] J. Koornneef, M. Spruijt, M. Molag, A. Ramirez, A. Faaij, and W. Turkenburg, "Uncertainties in risk assessment of CO2 pipelines," *Energy Procedia*, vol. 1, no. 1, pp. 1587–1594, Feb. 2009.

[3] Z. X. Zhang, G. X. Wang, P. Massarotto, and V. Rudolph, "Optimization of pipeline transport for CO2 sequestration," *Energy Convers. Manag.*, vol. 47, no. 6, pp. 702–715, Apr. 2006.

[4] P. Aursand, M. Hammer, S. T. Munkejord, and Ø. Wilhelmsen, "Pipeline transport of CO2 mixtures: Models for transient simulation," *Int. J. Greenh. Gas Control*, vol. 15, pp. 174–185, 2013.

[5] N. I. Diamantonis, G. C. Boulougouris, D. M. Tsangaris, M. J. El Kadi, H. Saadawi, S. Negahban, and I. G. Economou, "Thermodynamic and transport property models for carbon capture and sequestration (CCS) processes with emphasis on CO2 transport," *Chem. Eng. Res. Des.*, vol. 91, no. 10, pp. 1793–1806, 2013.

[6] R. T. J. Porter, M. Fairweather, M. Pourkashanian, and R. M. Woolley, "The range and level of impurities in CO2 streams from different carbon capture sources," *Int. J. Greenh. Gas Control*, vol. 36, pp. 161–174, May 2015.

[7] J.-Y. Lee, T. C. Keener, and Y. J. Yang, "Potential Flue Gas Impurities in Carbon Dioxide Streams Separated from Coal-Fired Power Plants," *J. Air Waste Manage. Assoc.*, vol. 59, no. 6, pp. 725–732, Feb. 2012.

[8] A. Kather and S. Kownatzki, "Assessment of the different parameters affecting the CO2 purity from coal fired oxyfuel process," *Int. J. Greenh. Gas Control*, vol. 5, pp. S204–S209, Jun. 2011.

[9] Y. Tan, W. Nookuea, H. Li, E. Thorin, L. Zhao, and J. Yan, "Property Impacts on Performance of CO2 Pipeline Transport," *Energy Procedia*, vol. 75, pp. 2261–2267, 2015.

[10] B. Wetenhall, H. Aghajani, H. Chalmers, S. D. Benson, M.-C. Ferrari, J. Li, J. M. Race, P. Singh, and J. Davison, "Impact of CO2 impurity on CO2 compression, liquefaction and transportation," *Energy Procedia*, vol. 63, pp. 2764–2778, 2014.

[11] Y. Tan, W. Nookuea, H. Li, E. Thorin, and J. Yan, "Property impacts on Carbon Capture and Storage (CCS) processes: A review," *Energy Convers. Manag.*, vol. 118, pp. 204–222, 2016.

[12] A. Chapoy, R. Burgass, B. Tohidi, and I. Alsiyabi, "Hydrate and Phase Behavior Modeling in CO2-Rich Pipelines," *J. Chem. Eng. Data*, vol. 60, no. 2, pp. 447–453, Feb. 2015.

[13] S.-S. Fan, G.-J. Chen, Q.-L. Ma, and T.-M. Guo, "Experimental and modeling studies on the hydrate formation of CO2 and CO2-rich gas mixtures," *Chem. Eng. J.*, vol. 78, no. 2, pp. 173–178, 2000.

[14] R. Span and W. Wagner, "A New Equation of State for Carbon Dioxide Covering the Fluid Region from the Triple-Point Temperature to 1100 K at Pressures up to 800 MPa," *J. Phys. Chem. Ref. Data*, vol. 25, no. 6, pp. 1509–1596, Nov. 1996.

[15] M. J. O. Kunz, R. Klimeck, W. Wagner, "GERG TECHNICAL MONOGRAPH 15, The GERG-2004 Wide-Range Equation of State for Natural Gases and Other Mixtures," 2007.

[16] H. Li and J. Yan, "Evaluating cubic equations of state for calculation of vapor–liquid equilibrium of CO2 and CO2-mixtures for CO2 capture and storage processes," *Appl. Energy*, vol. 86, no. 6, pp. 826–836, Jun. 2009.

[17] H. Li and J. Yan, "Impacts of equations of state (EOS) and impurities on the volume calculation of CO2 mixtures in the applications of CO2 capture and storage (CCS) processes," *Appl. Energy*, vol. 86, no. 12, pp. 2760–2770, Dec. 2009.

[18] G. Soave, "Equilibrium constants from a modified Redlich-Kwong equation of state," *Chem. Eng. Sci.*, vol. 27, no. 6, pp. 1197–1203, Jun. 1972.

[19] D.-Y. Peng and D. B. Robinson, "A New Two-Constant Equation of State," *Ind. Eng. Chem. Fundam.*, vol. 15, no. 1, pp. 59–64, Feb. 1976.

[20] A. Chapoy, M. Nazeri, M. Kapateh, R. Burgass, C. Coquelet, and B. Tohidi, "Effect of impurities on thermophysical properties and phase behaviour of a CO2-rich system in CCS," *Int. J. Greenh. Gas Control*, vol. 19, pp. 92–100, Nov. 2013.

[21] M. Nazeri, A. Chapoy, A. Valtz, C. Coquelet, and B. Tohidi, "Densities and derived thermophysical properties of the 0.9505 CO2+0.0495 H2S mixture from 273 K to 353 K and pressures up to 41 MPa," *Fluid Phase Equilib.*, vol. 423, pp. 156–171, Sep. 2016.

[22] A. Péneloux, E. Rauzy, and R. Fréze, "A consistent correction for Redlich-Kwong-Soave volumes," *Fluid Phase Equilib.*, vol. 8, no. 1, pp. 7–23, Jan. 1982.

[23] O. Kunz and W. Wagner, "The GERG-2008 Wide-Range Equation of State for Natural

Gases and Other Mixtures: An Expansion of GERG-2004," *J. Chem. Eng. Data*, vol. 57, no. 11, pp. 3032–3091, Nov. 2012.

[24] K. Frey, M. Modell, and J. W. Tester, "Density-and-temperature-dependent volume translation for the SRK EOS: 2. Mixtures," *Fluid Phase Equilib.*, vol. 343, pp. 13–23, 2013.

[25] R. Thiery, J. Vidal, and J. Dubessy, "Phase equilibria modelling applied to fluid inclusions: Liquid-vapour equilibria and calculation of the molar volume in the CO2□CH4□N2 system," *Geochim. Cosmochim. Acta*, vol. 58, no. 3, pp. 1073–1082, Feb. 1994.

[26] T. A. Al-Sahhaf, "Vapor—liquid equilibria for the ternary system N2 + CO2 + CH4 at 230 and 250 K," *Fluid Phase Equilib.*, vol. 55, no. 1–2, pp. 159–172, Jan. 1990.

[27] T. B. Boyle and J. J. Carroll, "Study determines best methods for calculating acid-gas density - Oil & Gas Journal," *Oil Gas J.*, vol. 100, no. 2, pp. 45–53, 2002.

[28] H. Li, J. P. Jakobsen, Ø. Wilhelmsen, and J. Yan, "PVTxy properties of CO2 mixtures relevant for CO2 capture, transport and storage: Review of available experimental data and theoretical models," *Appl. Energy*, vol. 88, no. 11, pp. 3567–3579, Nov. 2011.

[29] H. Li , "Thermodynamic properties of CO2 mixtures and their applications in advanced power cycles with CO2 capture processes," Department of chemical engineering and technology, Royal institute of technology, Stockholm, 2008.

[30] M. Mantovani, P. Chiesa, G. Valenti, M. Gatti, and S. Consonni, "Supercritical pressure–density–temperature measurements on CO2–N2, CO2–O2 and CO2–Ar binary mixtures," *J. Supercrit. Fluids*, vol. 61, pp. 34–43, Jan. 2012.

[31] Y. Sanchez-Vicente, T. C. Drage, M. Poliakoff, J. Ke, and M. W. George, "Densities of the carbon dioxide+hydrogen, a system of relevance to carbon capture and storage," *Int. J. Greenh. Gas Control*, vol. 13, pp. 78–86, 2013.

[32] C. Rivas, S. T. Blanco, J. Fernández, M. Artal, and I. Velasco, "Influence of methane and carbon monoxide in the volumetric behaviour of the anthropogenic CO2: Experimental data and modelling in the critical region," *Int. J. Greenh. Gas Control*, vol. 18, pp. 264–276, Oct. 2013.

[33] C. Coquelet, A. Valtz, F. Dieu, D. Richon, P. Arpentinier, and F. Lockwood, "Isothermal P, x, y data for the argon+carbon dioxide system at six temperatures from 233.32 to 299.21K and pressures up to 14MPa," *Fluid Phase Equilib.*, vol. 273, no. 1–2, pp. 38–43, Nov. 2008.

[34] O. Fandiño, J. P. M. Trusler, and D. Vega-Maza, "Phase behavior of (CO2+H2) and

(CO2+N2) at temperatures between (218.15 and 303.15)K at pressures up to 15MPa," *Int. J. Greenh. Gas Control*, vol. 36, pp. 78–92, May 2015.

[35] S. F. Westman, H. G. J. Stang, S. W. Løvseth, A. Austegard, I. Snustad, S. Ø. Størset, and I. S. Ertesvåg, "Vapor–liquid equilibrium data for the carbon dioxide and nitrogen (CO2 + N2) system at the temperatures 223, 270, 298 and 303 K and pressures up to 18 MPa," *Fluid Phase Equilib.*, vol. 409, pp. 207–241, 2016.

[36] S. F. Westman, H. G. J. Stang, S. W. Løvseth, A. Austegard, I. Snustad, and I. S. Ertesvåg, "Vapor-liquid equilibrium data for the carbon dioxide and oxygen (CO2 + O2) system at the temperatures 218, 233, 253, 273, 288 and 298 K and pressures up to 14 MPa," *Fluid Phase Equilib.*, vol. 421, pp. 67–87, Aug. 2016.

[37] X. Yang, M. Richter, M. A. Ben Souissi, R. Kleinrahm, and R. Span, "Vapor-Phase ( p , ρ, T, x ) Behavior and Virial Coefficients for the Binary Mixture (0.05 Argon + 0.95 Carbon Dioxide) over the Temperature Range from (273.15 to 323.15) K with Pressures up to 9 MPa," *J. Chem. Eng. Data*, vol. 61, no. 8, pp. 2676–2681, Aug. 2016.

[38] X. Yang, Z. Wang, and Z. Li, "Accurate Density Measurements on Ternary Mixtures (Carbon Dioxide + Nitrogen + Argon) at Temperatures from (323.15 to 423.15) K with Pressures from (3 to 31) MPa using a Single-Sinker Densimeter," *J. Chem. Eng. Data*, vol. 60, no. 11, pp. 3353–3357, Nov. 2015.

[39] B. Tohidi, R. W. Burgass, A. Danesh, and A. C. Todd, "Viscosity and Density of Methane + Methylcyclohexane from (323 to 423) K and Pressures to 140 MPa," *J. Chem. Eng. Data*, vol. 46, no. 2, pp. 385–390, Mar. 2001.

[40] E. W. Lemmon, M. L. Huber, and M. O. McLinden, "NIST standard reference database 23: reference fluid thermodynamic and transport properties – REFPROP version 8.0. Gaithersburg: National Institute of Standards and Technology, Standard Reference Data Program." 2007.

[41] I. Al-Siyabi, "Effect of Impurities on CO2 Stream Properties, PhD Thesis," Institute of Petroleum Engineering, Heriot-Watt University, Edinburgh, 2013.

[42] S. Bell, *Measurement Good Practice Guide No. 11 (Issue 2), A Beginner's Guide to Uncertainty of Measurement*. National Physical Laboratory, 2001.

[43] K. Kashefi, A. Chapoy, K. Bell, and B. Tohidi, "Viscosity of binary and multicomponent hydrocarbon fluids at high pressure and high temperature conditions: Measurements and predictions," *J. Pet. Sci. Eng.*, vol. 112, pp. 153–160, Dec. 2013.

[44] E. C. Efika, R. Hoballah, X. Li, E. F. May, M. Nania, Y. Sanchez-Vicente, and J. P. Martin Trusler, "Saturated phase densities of (CO2+H2O) at temperatures from (293 to

450)K and pressures up to 64MPa," *J. Chem. Thermodyn.*, vol. 93, pp. 347–359, Feb. 2016.

[45] G. S. Soave, "A Noncubic Equation of State for the Treatment of Hydrocarbon Fluids at Reservoir Conditions," *Ind. Eng. Chem. Res.*, vol. 34, no. 11, pp. 3981–3994, Nov. 1995.

[46] G. S. Soave, "An effective modification of the Benedict–Webb–Rubin equation of state," *Fluid Phase Equilib.*, vol. 164, no. 2, pp. 157–172, 1999.

[47] M. Benedict, G. B. Webb, and L. C. Rubin, "An Empirical Equation for Thermodynamic Properties of Light Hydrocarbons and Their Mixtures I. Methane, Ethane, Propane and n-Butane," *J. Chem. Phys.*, vol. 8, no. 4, p. 334, 1940.

[48] P. Ahmadi, A. Chapoy, and B. Tohidi, "Density, Speed of Sound and Derived Thermodynamic Properties of a Synthetic Natural Gas," *J. Nat. Gas Sci. Eng.*, 2016.

[49] A. G. Perez, A. Valtz, C. Coquelet, P. Paricaud, and A. Chapoy, "Experimental and modelling study of the densities of the hydrogen sulphide + methane mixtures at 253, 273 and 293 K and pressures up to 30 MPa," *Fluid Phase Equilib.*, vol. 427, pp. 371–383, 2016.

[50] L. M. C. Pereira, A. Chapoy, R. Burgass, and B. Tohidi, "Measurement and modelling of high pressure density and interfacial tension of (gas+n-alkane) binary mixtures," *J. Chem. Thermodyn.*, vol. 97, pp. 55–69, 2016.

[51] M. H. Kapateh, A. Chapoy, R. Burgass, and B. Tohidi, "Experimental Measurement and Modeling of the Solubility of Methane in Methanol and Ethanol," *J. Chem. Eng. Data*, vol. 61, no. 1, pp. 666–673, Jan. 2016.

[52] M. Wise, A. Chapoy, and R. Burgass, "Solubility Measurement and Modeling of Methane in Methanol and Ethanol Aqueous Solutions," *J. Chem. Eng. Data*, vol. 61, no. 9, pp. 3200–3207, Sep. 2016.

[53] M. Wise and A. Chapoy, "Carbon dioxide solubility in Triethylene Glycol and aqueous solutions," *Fluid Phase Equilib.*, vol. 419, pp. 39–49, 2016.

[54] A. Chapoy, M. Nazeri, M. Kapateh, R. Burgass, B. Tohidi, C. Coquelet, and P. Stingari, "Impact of CommonImpurities on CO2 Capture, Transport and Storage, 2011-2014 Programme, Final Report," 2015.

Table 1. Compositions of the multi-component mixtures along with the corresponding expanded uncertainties (coverage factor *k=2*) in the parentheses

| Components | MIX 1 / mol% | MIX 2 / mol% | MIX 3 / mol% |
|---|---|---|---|
| Carbon Dioxide | 95.6437 | 89.83 | 69.99 |
| Methane | 0.6261 (0.031) | 0 | 20.02 (0.11) |
| Ethane | 0 | 0 | 6.612 (0.034) |
| Propane | 0 | 0 | 2.58 (0.013) |
| n-Butane | 0 | 0 | 0.3997 (40 ppm) |
| i-Butane | 0 | 0 | 0.3998 (40 ppm) |
| Nitrogen | 1.41 (0.071) | 5.05 (0.04) | 0 |
| Hydrogen | 0.8175 (0.041) | 0 | 0 |
| Oxygen | 0.08 (0.004) | 3.07 (0.10) | 0 |
| Argon | 1.21 (0.061) | 2.05 (0.06) | 0 |
| Carbon Monoxide | 0.2127 (0.011) | 0 | 0 |
| Total | 100.00 | 100.00 | 100.00 |
| Certification | BOC | BOC | BOC |
| Analysis Method | SM [a] | SM [a] | SM [a] |

[a] Supplier Method: The analysis techniques was based on the gas chromatography using flame ionization detector and thermal conductivity detector.

Table 2. Calibration data using pure $CO_2$ at low pressures (gas phase)

| No | $T$/K | $p$/MPa | $\tau$/μs | $\rho_{REF}$/g.cm$^{-3}$ [40] | $\tau^2$/μs$^2$ |
|---|---|---|---|---|---|
| 1 | 273.3 | 1.28 | 2417.372 | 0.0272 | 5843687.4 |
| 2 | 273.3 | 2.08 | 2419.303 | 0.0477 | 5853027.0 |
| 3 | 273.3 | 3.29 | 2423.028 | 0.0887 | 5871064.7 |
| 4 | 283.3 | 0.97 | 2420.026 | 0.0192 | 5856525.8 |
| 5 | 283.3 | 2.08 | 2422.275 | 0.0451 | 5867416.2 |
| 6 | 283.3 | 3.81 | 2427.179 | 0.0999 | 5891197.9 |
| 7 | 283.3 | 0.74 | 2419.422 | 0.0146 | 5853602.8 |
| 8 | 283.3 | 0.99 | 2419.942 | 0.0196 | 5856119.3 |
| 9 | 283.3 | 2.03 | 2422.182 | 0.0438 | 5866965.6 |
| 10 | 283.3 | 4.11 | 2428.783 | 0.1133 | 5898986.9 |
| 11 | 298.4 | 0.67 | 2423.921 | 0.0123 | 5875393.0 |
| 12 | 298.4 | 1.03 | 2424.438 | 0.0194 | 5877899.6 |
| 13 | 298.4 | 2.08 | 2426.469 | 0.0415 | 5887751.8 |
| 14 | 298.4 | 5.17 | 2435.391 | 0.1387 | 5931129.3 |
| 15 | 323.5 | 1.04 | 2432.229 | 0.0177 | 5915737.9 |
| 16 | 323.5 | 1.70 | 2433.385 | 0.0299 | 5921362.6 |
| 17 | 323.5 | 2.10 | 2434.084 | 0.0374 | 5924764.9 |
| 18 | 323.5 | 5.23 | 2440.921 | 0.1112 | 5958095.3 |
| 19 | 323.5 | 6.92 | 2446.297 | 0.1682 | 5984369.0 |
| 20 | 373.6 | 1.05 | 2448.685 | 0.0153 | 5996058.2 |
| 21 | 373.6 | 1.32 | 2449.071 | 0.0193 | 5997948.8 |
| 22 | 373.6 | 2.08 | 2450.061 | 0.0310 | 6002798.9 |
| 23 | 373.6 | 5.20 | 2455.071 | 0.0842 | 6027373.6 |
| 24 | 373.6 | 10.49 | 2466.093 | 0.2006 | 6081614.7 |
| 25 | 423.5 | 1.31 | 2465.475 | 0.0167 | 6078567.0 |
| 26 | 423.5 | 2.08 | 2466.363 | 0.0268 | 6082946.4 |
| 27 | 423.5 | 4.98 | 2470.217 | 0.0671 | 6101972.0 |
| 28 | 423.5 | 10.38 | 2478.314 | 0.1517 | 6142040.3 |
| 29 | 423.5 | 20.82 | 2497.709 | 0.3415 | 6238550.2 |

The standard uncertainty for the temperature, pressure and period are:
$u(T)$ = 0.02 K, $u(p)$ = 0.02 MPa and $u(\tau)$ = 0.005 μs

Table 3. Calibration data using pure $CO_2$ at high pressures (dense phase)

| No | $T$/K | $p$/MPa | $\tau$/μs | $\rho_{REF}$/g.cm$^{-3}$ [40] | $\tau^2$/μs$^2$ |
|---|---|---|---|---|---|
| 1 | 273.1 | 3.61 | 2500.031 | 0.9292 | 6250155.0 |
| 2 | 273.1 | 4.96 | 2500.974 | 0.9407 | 6254870.9 |
| 3 | 273.1 | 10.76 | 2504.517 | 0.9786 | 6272605.4 |
| 4 | 273.1 | 20.94 | 2508.752 | 1.0243 | 6293836.6 |
| 5 | 273.1 | 52.06 | 2516.628 | 1.1088 | 6333416.5 |
| 6 | 273.1 | 103.63 | 2524.503 | 1.1907 | 6373115.4 |
| 7 | 273.1 | 125.17 | 2527.011 | 1.2161 | 6385784.6 |
| 8 | 283.0 | 4.60 | 2497.442 | 0.8637 | 6237216.5 |
| 9 | 283.0 | 5.20 | 2497.982 | 0.8724 | 6239914.1 |
| 10 | 283.0 | 10.48 | 2502.835 | 0.9249 | 6264183.0 |
| 11 | 283.0 | 21.33 | 2508.552 | 0.9868 | 6292833.1 |
| 12 | 283.0 | 51.44 | 2517.232 | 1.0803 | 6336456.9 |
| 13 | 283.0 | 104.13 | 2525.886 | 1.1707 | 6380100.1 |
| 14 | 283.0 | 125.56 | 2528.511 | 1.1973 | 6393367.9 |
| 15 | 298.5 | 4.99 | 2434.706 | 0.1304 | 5927793.3 |
| 16 | 298.5 | 12.34 | 2500.926 | 0.8472 | 6254630.9 |
| 17 | 298.5 | 20.40 | 2507.222 | 0.9152 | 6286162.2 |
| 18 | 298.5 | 50.96 | 2518.404 | 1.0358 | 6342358.7 |
| 19 | 298.5 | 76.41 | 2523.778 | 1.0928 | 6369455.4 |
| 20 | 298.5 | 103.65 | 2528.125 | 1.1380 | 6391416.0 |
| 21 | 298.5 | 124.91 | 2530.945 | 1.1668 | 6405682.6 |
| 22 | 298.5 | 22.90 | 2508.612 | 0.9302 | 6293134.2 |
| 23 | 323.7 | 40.12 | 2516.382 | 0.9221 | 6332178.4 |
| 24 | 323.7 | 25.52 | 2508.396 | 0.8361 | 6292050.5 |
| 25 | 323.7 | 76.90 | 2526.968 | 1.0352 | 6385567.3 |
| 26 | 323.7 | 104.17 | 2531.985 | 1.0878 | 6410948.0 |
| 27 | 323.7 | 125.53 | 2535.163 | 1.1205 | 6427051.4 |
| 28 | 323.7 | 125.53 | 2535.163 | 1.1205 | 6427051.4 |
| 29 | 373.5 | 17.16 | 2489.108 | 0.3984 | 6195658.6 |
| 30 | 373.5 | 20.84 | 2493.806 | 0.5002 | 6219068.4 |
| 31 | 373.5 | 35.63 | 2514.401 | 0.7198 | 6322212.4 |
| 32 | 373.5 | 52.12 | 2524.656 | 0.8286 | 6373887.9 |
| 33 | 373.5 | 104.28 | 2540.168 | 0.9914 | 6452453.5 |
| 34 | 373.5 | 125.86 | 2544.158 | 1.0325 | 6472739.9 |
| 35 | 423.4 | 26.99 | 2506.068 | 0.4470 | 6280376.8 |
| 36 | 423.4 | 51.34 | 2529.613 | 0.6953 | 6398941.9 |
| 37 | 423.4 | 75.91 | 2541.127 | 0.8158 | 6457326.4 |
| 38 | 423.4 | 104.24 | 2549.567 | 0.9024 | 6500291.9 |
| 39 | 423.4 | 124.66 | 2554.176 | 0.9487 | 6523815.0 |

The standard uncertainty for the temperature, pressure and period are:
$u(T)$ = 0.02 K, $u(p)$ = 0.02 MPa and $u(\tau)$ = 0.005 μs

Table 4. Calibration Parameters for Anton Paar DMA-HPM Densitometer using pure $CO_2$

| | Gas Phase | | Liquid or Supercritical Phase | |
|---|---|---|---|---|
| *T* / K | *A* | *B* | *A* | *B* |
| 273.2 | 2.2489E-06 | 13.1148729 | 2.11433E-06 | 12.28403271 |
| 283.2 | 2.22815E-06 | 13.02872592 | 2.13096E-06 | 12.42475544 |
| 298.2 | 2.25362E-06 | 13.22771299 | 2.11904E-06 | 12.40548964 |
| 323.2 | 2.19724E-06 | 12.98059669 | 2.10897E-06 | 12.43289764 |
| 373.2 | 2.16346E-06 | 12.95646413 | 2.09829E-06 | 12.54758176 |
| 423.2 | 2.02721E-06 | 12.30358989 | 2.06409E-06 | 12.51471964 |

Table 5. Modified binary interaction parameters in this work for PR EoS [54]

| | $CO_2$ | CO | $N_2$ | $O_2$ | Ar | $H_2$ | $CH_4$ | $C_2H_6$ | $C_3H_8$ | $SO_2$ | $H_2S$ |
|---|---|---|---|---|---|---|---|---|---|---|---|
| $CO_2$ | | -0.079 | -0.014 | 0.111 | 0.129 | 0.089 | 0.099 | 0.129 | 0.131 | 0.02 | 0.082 |
| CO | | | 0.005 | 0[a] | 0.007 | 0[a] | 0.022 | -0.003 | 0[a] | 0.024 | 0.085 |
| $N_2$ | | | | -0.013 | -0.007 | 0[a] | 0.032 | 0.039 | 0.083 | 0.128 | 0.174 |
| $O_2$ | | | | | 0[a] | 0[a] | 0[a] | 0[a] | 0.112 | 0.222 | 0[a] |
| Ar | | | | | | 0[a] | 0.026 | 0.054 | 0[a] | 0[a] | 0[a] |
| $H_2$ | | | | | | | 0[a] | 0[a] | 0[a] | 0[a] | 0[a] |
| $CH_4$ | | | | | | | | 0.001 | 0.016 | 0.129 | 0.084 |
| $C_2H_6$ | | | | | | | | | -0.006 | 0.11 | 0.084 |
| $C_3H_8$ | | | | | | | | | | 0[a] | 0.082 |
| $SO_2$ | | | | | | | | | | | 0[a] |
| $H_2S$ | | | | | | | | | | | |

a The EoS was not tuned for this binary system

Table 6. Modified binary interaction parameters in this work for SRK EoS [54]

| | $CO_2$ | CO | $N_2$ | $O_2$ | Ar | $H_2$ | $CH_4$ | $C_2H_6$ | $C_3H_8$ | $SO_2$ | $H_2S$ |
|---|---|---|---|---|---|---|---|---|---|---|---|
| $CO_2$ | | -0.062 | -0.046 | 0.106 | 0.123 | 0.2 | 0.100 | 0.137 | 0.139 | 0.020 | 0.096 |
| CO | | | 0.006 | 0[a] | 0.008 | 0[a] | 0.030 | -0.022 | 0[a] | 0.000 | 0.061 |
| $N_2$ | | | | -0.014 | -0.008 | 0[a] | 0.030 | 0.032 | 0.078 | 0.091 | 0.157 |
| $O_2$ | | | | | 0[a] | 0[a] | 0[a] | 0[a] | 0.113 | 0.219 | 0[a] |
| Ar | | | | | | 0[a] | 0.028 | 0.053 | 0[a] | 0[a] | 0[a] |
| $H_2$ | | | | | | | 0[a] | 0[a] | 0[a] | 0[a] | 0[a] |
| $CH_4$ | | | | | | | | -0.003 | 0.010 | 0.119 | 0.077 |
| $C_2H_6$ | | | | | | | | | -0.005 | 0.11 | 0.087 |
| $C_3H_8$ | | | | | | | | | | 0[a] | 0.087 |
| $SO_2$ | | | | | | | | | | | 0[a] |
| $H_2S$ | | | | | | | | | | | |

a The EoS was not tuned for this binary system

Table 7. Experimental and modeling results of MIX 1

| Phase | $T$/K | $p$/MPa | $\rho_{exp}$/ kg.m$^{-3}$ | $u_c(\rho)$/ kg.m$^{-3}$ | $\rho_{model}$/kg.m$^{-3}$ | | | | $(\rho_{exp}-\rho_{model})/\rho_{exp} \times 100$ | | | |
|---|---|---|---|---|---|---|---|---|---|---|---|---|
| | | | | | PR-$CO_2$ | PR | PR-Pen | GERG | PR-$CO_2$ | PR | PR-Pen | GERG |
| Gas | 273.4 | 1.71 | 38.4 | 0.5 | 37.7 | 37.6 | 37.6 | 36.7 | 2.0 | 2.1 | 2.2 | 4.4 |
| Gas | 273.4 | 2.07 | 47.4 | 0.5 | 47.1 | 47.0 | 46.9 | 45.8 | 0.6 | 0.7 | 0.9 | 3.3 |
| Gas | 273.4 | 2.73 | 66.4 | 0.6 | 66.6 | 66.5 | 66.3 | 64.5 | 0.3 | 0.2 | 0.1 | 2.8 |
| Liq. | 273.4 | 6.71 | 888.0 | 3.3 | 894.0 | 893.8 | 859.8 | 881.8 | 0.7 | 0.6 | 3.2 | 0.7 |
| Liq. | 273.4 | 11.31 | 927.8 | 2.7 | 937.2 | 950.6 | 912.3 | 920.8 | 1.0 | 2.5 | 1.7 | 0.8 |
| Liq. | 273.4 | 21.80 | 983.9 | 2.2 | 997.9 | 1032.0 | 987.0 | 977.2 | 1.4 | 4.9 | 0.3 | 0.7 |
| Liq. | 273.4 | 36.27 | 1034.2 | 2.0 | 1051.3 | 1102.1 | 1050.8 | 1027.7 | 1.7 | 6.6 | 1.6 | 0.6 |
| Liq. | 273.4 | 51.73 | 1073.6 | 1.8 | 1092.6 | 1153.9 | 1097.9 | 1067.1 | 1.8 | 7.5 | 2.3 | 0.6 |
| Liq. | 273.4 | 76.40 | 1121.7 | 1.7 | 1142.2 | 1212.6 | 1150.9 | 1114.7 | 1.8 | 8.1 | 2.6 | 0.6 |
| Liq. | 273.4 | 104.38 | 1164.4 | 1.6 | 1185.1 | 1260.3 | 1193.8 | 1156.5 | 1.8 | 8.2 | 2.5 | 0.7 |
| Liq. | 273.4 | 126.02 | 1192.1 | 1.6 | 1211.9 | 1288.9 | 1219.4 | 1183.4 | 1.7 | 8.1 | 2.3 | 0.7 |
| Gas | 283.3 | 1.81 | 37.6 | 0.5 | 38.0 | 38.0 | 38.0 | 37.1 | 1.1 | 1.1 | 0.9 | 1.4 |
| Gas | 283.3 | 3.37 | 80.4 | 0.7 | 82.1 | 81.6 | 81.3 | 78.8 | 2.1 | 1.5 | 1.1 | 2.0 |
| Liq. | 283.3 | 6.36 | 810.8 | 0.7 | 797.9 | 778.3 | 752.4 | 821.4 | 1.6 | 4.0 | 7.2 | 1.3 |
| Liq. | 283.3 | 11.68 | 888.9 | 3.0 | 881.9 | 882.9 | 849.7 | 867.3 | 0.8 | 0.7 | 4.4 | 2.4 |
| Liq. | 283.3 | 22.57 | 956.3 | 2.3 | 960.9 | 987.7 | 946.4 | 941.0 | 0.5 | 3.3 | 1.0 | 1.6 |
| Liq. | 283.3 | 36.41 | 1004.6 | 2.0 | 1019.4 | 1065.2 | 1017.3 | 996.7 | 1.5 | 6.0 | 1.3 | 0.8 |
| Liq. | 283.3 | 54.13 | 1052.1 | 1.8 | 1070.7 | 1130.6 | 1076.8 | 1045.9 | 1.8 | 7.5 | 2.3 | 0.6 |
| Liq. | 283.3 | 78.00 | 1099.3 | 1.7 | 1121.2 | 1191.4 | 1131.8 | 1094.5 | 2.0 | 8.4 | 3.0 | 0.4 |
| Liq. | 283.3 | 105.09 | 1141.3 | 1.6 | 1164.8 | 1240.9 | 1176.3 | 1137.1 | 2.1 | 8.7 | 3.1 | 0.4 |
| Liq. | 283.3 | 124.85 | 1167.1 | 1.5 | 1190.8 | 1269.0 | 1201.6 | 1162.9 | 2.0 | 8.7 | 3.0 | 0.4 |
| Gas | 298.3 | 1.68 | 32.1 | 0.4 | 32.3 | 32.6 | 32.5 | 31.8 | 0.6 | 1.4 | 1.3 | 1.0 |
| Gas | 298.3 | 1.96 | 38.6 | 0.4 | 38.3 | 38.7 | 38.6 | 37.7 | 0.7 | 0.3 | 0.1 | 2.3 |
| Gas | 298.3 | 2.76 | 57.0 | 0.5 | 56.7 | 57.5 | 57.4 | 55.8 | 0.5 | 0.9 | 0.6 | 2.2 |
| Gas | 298.3 | 3.08 | 64.8 | 0.5 | 64.6 | 65.6 | 65.4 | 63.5 | 0.3 | 1.3 | 1.0 | 2.0 |
| Liq. | 298.3 | 12.55 | 778.4 | 3.6 | 784.9 | 767.0 | 741.9 | 772.8 | 0.8 | 1.5 | 4.7 | 0.7 |
| Liq. | 298.4 | 20.26 | 865.2 | 2.5 | 876.0 | 883.0 | 849.8 | 859.0 | 1.2 | 2.1 | 1.8 | 0.7 |
| Liq. | 298.4 | 50.12 | 999.6 | 1.8 | 1016.8 | 1068.2 | 1020.0 | 993.8 | 1.7 | 6.9 | 2.0 | 0.6 |
| Liq. | 298.4 | 75.62 | 1061.8 | 1.6 | 1080.1 | 1147.4 | 1092.0 | 1055.1 | 1.7 | 8.1 | 2.8 | 0.6 |
| Liq. | 298.4 | 103.39 | 1111.8 | 1.6 | 1130.0 | 1206.0 | 1144.9 | 1103.7 | 1.6 | 8.5 | 3.0 | 0.7 |
| Liq. | 298.4 | 126.33 | 1145.6 | 1.5 | 1162.8 | 1242.5 | 1177.8 | 1136.1 | 1.5 | 8.5 | 2.8 | 0.8 |
| Gas | 323.4 | 1.45 | 24.0 | 0.4 | 24.9 | 25.1 | 25.1 | 24.6 | 4.0 | 4.7 | 4.6 | 2.4 |
| Gas | 323.4 | 2.19 | 37.4 | 0.4 | 38.8 | 39.1 | 39.1 | 38.2 | 3.7 | 4.7 | 4.5 | 2.1 |
| Gas | 323.3 | 3.60 | 66.0 | 0.5 | 68.0 | 69.1 | 68.9 | 66.9 | 3.1 | 4.7 | 4.4 | 1.4 |
| Gas | 323.3 | 5.22 | 104.6 | 0.6 | 107.4 | 109.9 | 109.3 | 105.5 | 2.8 | 5.1 | 4.6 | 0.9 |
| Gas | 323.4 | 8.27 | 209.5 | 1.3 | 213.8 | 219.1 | 217.0 | 208.3 | 2.0 | 4.5 | 3.5 | 0.6 |
| SC | 323.4 | 15.88 | 642.4 | 3.8 | 649.7 | 617.0 | 600.7 | 633.5 | 1.1 | 3.9 | 6.5 | 1.4 |
| SC | 323.4 | 22.59 | 758.5 | 2.6 | 767.8 | 756.9 | 732.3 | 752.9 | 1.2 | 0.2 | 3.4 | 0.7 |
| SC | 323.4 | 29.52 | 822.1 | 2.2 | 833.7 | 840.6 | 810.5 | 817.2 | 1.4 | 2.3 | 1.4 | 0.6 |
| SC | 323.4 | 54.07 | 941.5 | 1.7 | 957.5 | 1001.4 | 958.9 | 936.8 | 1.7 | 6.4 | 1.9 | 0.5 |
| SC | 323.4 | 77.97 | 1008.7 | 1.6 | 1026.1 | 1088.4 | 1038.4 | 1003.1 | 1.7 | 7.9 | 2.9 | 0.6 |
| SC | 323.4 | 106.00 | 1065.5 | 1.5 | 1082.7 | 1157.1 | 1100.8 | 1058.3 | 1.6 | 8.6 | 3.3 | 0.7 |
| SC | 323.4 | 126.46 | 1099.1 | 1.5 | 1115.2 | 1194.9 | 1135.0 | 1090.4 | 1.5 | 8.7 | 3.3 | 0.8 |
| Gas | 373.5 | 2.12 | 29.1 | 0.3 | 31.3 | 31.5 | 31.4 | 30.8 | 7.7 | 8.4 | 8.3 | 6.1 |
| Gas | 373.5 | 2.75 | 40.2 | 0.3 | 41.3 | 41.6 | 41.5 | 40.6 | 2.8 | 3.6 | 3.4 | 1.2 |
| Gas | 373.5 | 3.52 | 50.3 | 0.3 | 53.7 | 54.2 | 54.1 | 52.8 | 6.6 | 7.7 | 7.4 | 5.0 |
| Gas | 373.5 | 5.24 | 79.9 | 0.4 | 83.6 | 84.7 | 84.4 | 82.2 | 4.6 | 6.0 | 5.6 | 2.9 |
| Gas | 373.5 | 10.61 | 191.4 | 0.7 | 196.2 | 198.3 | 196.6 | 192.4 | 2.5 | 3.6 | 2.7 | 0.5 |
| SC | 373.5 | 26.16 | 568.5 | 2.0 | 576.2 | 554.8 | 541.5 | 561.1 | 1.3 | 2.4 | 4.7 | 1.3 |
| SC | 373.5 | 53.57 | 805.3 | 1.6 | 815.5 | 836.6 | 806.8 | 799.8 | 1.3 | 3.9 | 0.2 | 0.7 |
| SC | 373.5 | 77.94 | 900.8 | 1.5 | 912.6 | 959.0 | 920.0 | 893.7 | 1.3 | 6.5 | 2.1 | 0.8 |
| SC | 373.6 | 104.58 | 970.6 | 1.4 | 982.9 | 1046.3 | 1000.1 | 961.4 | 1.3 | 7.8 | 3.0 | 1.0 |
| SC | 373.6 | 123.18 | 1008.7 | 1.4 | 1020.6 | 1092.1 | 1041.7 | 997.9 | 1.2 | 8.3 | 3.3 | 1.1 |
| Gas | 423.4 | 0.95 | 11.4 | 0.3 | 11.9 | 12.0 | 12.0 | 11.8 | 4.6 | 4.7 | 4.7 | 3.0 |

| | | | | | | | | | | | | |
|---|---|---|---|---|---|---|---|---|---|---|---|---|
| Gas | 423.4 | 2.09 | 25.3 | 0.3 | 26.7 | 26.8 | 26.7 | 26.2 | 5.2 | 5.6 | 5.4 | 3.6 |
| Gas | 423.4 | 3.59 | 44.5 | 0.3 | 46.9 | 47.2 | 47.1 | 46.2 | 5.4 | 5.9 | 5.7 | 3.7 |
| Gas | 423.4 | 5.28 | 66.8 | 0.3 | 70.6 | 71.0 | 70.8 | 69.4 | 5.6 | 6.3 | 5.9 | 3.9 |
| Gas | 423.4 | 7.74 | 101.7 | 0.3 | 107.2 | 107.9 | 107.4 | 105.3 | 5.4 | 6.1 | 5.6 | 3.6 |
| SC | 423.4 | 34.18 | 521.3 | 1.3 | 527.1 | 514.5 | 503.0 | 515.3 | 1.1 | 1.3 | 3.5 | 1.1 |
| SC | 423.4 | 53.52 | 682.4 | 1.4 | 692.0 | 697.6 | 676.7 | 678.6 | 1.4 | 2.2 | 0.8 | 0.5 |
| SC | 423.4 | 76.14 | 791.7 | 1.3 | 803.6 | 832.9 | 803.3 | 787.7 | 1.5 | 5.2 | 1.5 | 0.5 |
| SC | 423.4 | 104.16 | 880.1 | 1.3 | 894.1 | 944.2 | 906.3 | 874.6 | 1.6 | 7.3 | 3.0 | 0.6 |
| SC | 423.4 | 121.85 | 922.5 | 1.2 | 937.2 | 996.5 | 954.5 | 915.7 | 1.6 | 8.0 | 3.5 | 0.7 |
| | | | | | *AAD* / % | | | | 2.1 | 4.9 | 3.0 | 1.5 |

The standard uncertainty for the temperature, pressure and period are:
$u(T)$ = 0.02 K, $u(p)$ = 0.02 MPa and $u(\tau)$ = 0.005 μs

Table 8. Experimental and modeling results of MIX 2

| Phase | $T$/K | $p$/MPa | $\rho_{exp}$/ kg.m$^{-3}$ | $u_c(\rho)$/ kg.m$^{-3}$ | $\rho_{model}$/kg.m$^{-3}$ | | | | $(\rho_{exp}-\rho_{model})/\rho_{exp}\times 100$ | | | |
|---|---|---|---|---|---|---|---|---|---|---|---|---|
| | | | | | PR-CO$_2$ | PR | PR-Pen | GERG | PR-CO$_2$ | PR | PR-Pen | GERG |
| Gas | 273.2 | 1.79 | 38.4 | 0.5 | 38.4 | 38.3 | 38.2 | 37.9 | 0.2 | 0.3 | 0.7 | 1.4 |
| Gas | 273.2 | 2.24 | 49.8 | 0.5 | 50.0 | 50.0 | 49.7 | 49.3 | 0.5 | 0.3 | 0.1 | 1.0 |
| Liq. | 273.3 | 8.80 | 841.6 | 2.6 | 837.4 | 842.8 | 810.0 | 846.5 | 0.5 | 0.1 | 3.8 | 0.6 |
| Liq. | 273.3 | 10.92 | 867.7 | 2.2 | 865.7 | 876.1 | 840.8 | 871.0 | 0.2 | 1.0 | 3.1 | 0.4 |
| Liq. | 273.3 | 21.00 | 941.0 | 1.5 | 947.2 | 975.8 | 932.2 | 942.9 | 0.7 | 3.7 | 0.9 | 0.2 |
| Liq. | 273.3 | 52.04 | 1048.9 | 1.0 | 1064.0 | 1119.6 | 1062.7 | 1050.3 | 1.4 | 6.7 | 1.3 | 0.1 |
| Liq. | 273.3 | 104.16 | 1145.6 | 0.7 | 1163.2 | 1232.4 | 1163.9 | 1145.2 | 1.5 | 7.6 | 1.6 | 0.0 |
| Liq. | 273.3 | 125.71 | 1174.9 | 0.7 | 1191.4 | 1262.6 | 1190.8 | 1173.5 | 1.4 | 7.5 | 1.4 | 0.1 |
| Gas | 283.3 | 1.74 | 37.0 | 0.5 | 35.0 | 35.3 | 35.2 | 34.9 | 5.4 | 4.6 | 5.0 | 5.7 |
| Gas | 283.3 | 2.28 | 46.5 | 0.5 | 48.3 | 48.0 | 47.8 | 47.4 | 3.8 | 3.2 | 2.7 | 1.8 |
| Liq. | 283.3 | 10.67 | 803.7 | 2.9 | 783.5 | 781.6 | 753.2 | 793.6 | 2.5 | 2.7 | 6.3 | 1.3 |
| Liq. | 283.3 | 20.84 | 895.0 | 1.6 | 899.0 | 919.2 | 880.4 | 896.9 | 0.5 | 2.7 | 1.6 | 0.2 |
| Liq. | 283.3 | 52.46 | 1012.6 | 1.0 | 1036.0 | 1089.0 | 1035.1 | 1023.3 | 2.3 | 7.5 | 2.2 | 1.1 |
| Liq. | 283.3 | 104.12 | 1114.4 | 0.7 | 1141.3 | 1211.2 | 1144.9 | 1124.1 | 2.4 | 8.7 | 2.7 | 0.9 |
| Liq. | 283.3 | 125.26 | 1145.3 | 0.7 | 1170.9 | 1243.1 | 1173.4 | 1153.4 | 2.2 | 8.5 | 2.5 | 0.7 |
| Gas | 298.4 | 2.08 | 39.2 | 0.4 | 39.7 | 40.1 | 39.9 | 39.6 | 1.1 | 2.1 | 1.7 | 0.8 |
| Gas | 298.4 | 3.53 | 75.3 | 0.5 | 73.5 | 74.7 | 74.3 | 73.2 | 2.4 | 0.8 | 1.4 | 2.8 |
| SC | 298.4 | 12.58 | 702.1 | 3.5 | 684.0 | 670.9 | 649.5 | 693.6 | 2.6 | 4.4 | 7.5 | 1.2 |
| SC | 298.4 | 20.81 | 827.0 | 1.8 | 820.8 | 827.7 | 795.9 | 821.8 | 0.7 | 0.1 | 3.8 | 0.6 |
| SC | 298.4 | 51.34 | 979.9 | 1.0 | 988.3 | 1035.2 | 986.3 | 977.5 | 0.9 | 5.6 | 0.7 | 0.2 |
| SC | 298.4 | 104.10 | 1097.0 | 0.7 | 1108.9 | 1178.7 | 1115.9 | 1093.1 | 1.1 | 7.5 | 1.7 | 0.4 |
| SC | 298.4 | 125.88 | 1130.3 | 0.7 | 1141.8 | 1215.2 | 1148.5 | 1125.4 | 1.0 | 7.5 | 1.6 | 0.4 |
| Gas | 323.5 | 2.57 | 45.3 | 0.4 | 45.0 | 45.4 | 45.3 | 44.9 | 0.7 | 0.4 | 0.0 | 0.9 |
| Gas | 323.5 | 3.70 | 67.5 | 0.4 | 67.8 | 68.8 | 68.4 | 67.6 | 0.3 | 1.9 | 1.3 | 0.1 |
| SC | 323.5 | 12.27 | 409.1 | 2.7 | 406.6 | 383.8 | 375.8 | 387.6 | 0.6 | 6.2 | 8.1 | 5.3 |
| SC | 323.5 | 20.91 | 687.5 | 2.1 | 677.9 | 665.0 | 643.9 | 679.9 | 1.4 | 3.3 | 6.3 | 1.1 |
| SC | 323.5 | 51.56 | 909.3 | 1.0 | 914.3 | 950.9 | 909.3 | 906.7 | 0.5 | 4.6 | 0.0 | 0.3 |
| SC | 323.5 | 105.06 | 1047.7 | 0.7 | 1058.2 | 1126.1 | 1068.5 | 1044.5 | 1.0 | 7.5 | 2.0 | 0.3 |
| SC | 323.5 | 125.48 | 1082.4 | 0.7 | 1092.9 | 1166.0 | 1104.4 | 1078.4 | 1.0 | 7.7 | 2.0 | 0.4 |
| Gas | 373.6 | 1.53 | 20.7 | 0.3 | 21.7 | 21.8 | 21.8 | 21.7 | 4.7 | 5.2 | 4.9 | 4.6 |
| Gas | 373.6 | 2.57 | 34.5 | 0.3 | 37.3 | 37.6 | 37.4 | 37.2 | 8.1 | 8.8 | 8.4 | 7.9 |
| SC | 373.5 | 17.22 | 353.9 | 1.0 | 346.3 | 337.6 | 331.6 | 341.5 | 2.2 | 4.6 | 6.3 | 3.5 |
| SC | 373.5 | 21.00 | 439.7 | 1.2 | 435.9 | 419.7 | 410.7 | 429.6 | 0.9 | 4.6 | 6.6 | 2.3 |
| SC | 373.5 | 52.56 | 777.7 | 1.0 | 776.8 | 794.1 | 764.6 | 773.5 | 0.1 | 2.1 | 1.7 | 0.5 |
| SC | 373.6 | 103.94 | 951.8 | 0.7 | 958.3 | 1015.8 | 968.5 | 947.7 | 0.7 | 6.7 | 1.8 | 0.4 |
| SC | 373.6 | 125.15 | 996.1 | 0.6 | 1003.1 | 1069.3 | 1017.1 | 990.9 | 0.7 | 7.4 | 2.1 | 0.5 |
| Gas | 423.5 | 2.40 | 30.4 | 0.3 | 30.0 | 30.1 | 30.0 | 29.9 | 1.2 | 0.8 | 1.2 | 1.4 |
| Gas | 423.5 | 3.41 | 43.6 | 0.3 | 43.3 | 43.5 | 43.3 | 43.2 | 0.6 | 0.1 | 0.5 | 0.8 |
| SC | 423.4 | 18.47 | 283.7 | 0.5 | 273.7 | 270.5 | 266.5 | 272.3 | 3.5 | 4.7 | 6.1 | 4.0 |
| SC | 423.4 | 21.75 | 335.5 | 0.6 | 327.0 | 320.8 | 315.4 | 324.9 | 2.5 | 4.4 | 6.0 | 3.2 |
| SC | 423.4 | 52.79 | 660.6 | 0.8 | 657.9 | 662.1 | 641.3 | 655.5 | 0.4 | 0.2 | 2.9 | 0.8 |
| SC | 423.4 | 102.77 | 862.5 | 0.6 | 867.4 | 912.0 | 873.5 | 858.9 | 0.6 | 5.7 | 1.3 | 0.4 |
| SC | 423.4 | 124.65 | 915.9 | 0.6 | 922.2 | 977.5 | 933.5 | 911.1 | 0.7 | 6.7 | 1.9 | 0.5 |
| | | | | *AAD* / % | | | | | 1.6 | 4.3 | 2.9 | 1.4 |

The standard uncertainty for the temperature, pressure and period are:
$u(T)$ = 0.02 K, $u(p)$ = 0.02 MPa and $u(\tau)$ = 0.005 μs

Table 9. Experimental and modeling results of MIX 3

| Phase | $T$/K | $p$/MPa | $\rho_{exp}$/ kg.m$^{-3}$ | $u_c(\rho)$/ kg.m$^{-3}$ | $\rho_{model}$/kg.m$^{-3}$ | | | | $(\rho_{exp}-\rho_{model})/\rho_{exp} \times 100$ | | | |
|---|---|---|---|---|---|---|---|---|---|---|---|---|
| | | | | | PR-$CO_2$ | PR | PR-Pen | GERG | PR-$CO_2$ | PR | PR-Pen | GERG |
| Gas | 273.3 | 1.07 | 20.0 | 0.4 | 19.0 | 19.0 | 19.0 | 18.9 | 4.8 | 4.8 | 5.0 | 5.5 |
| Gas | 273.3 | 2.13 | 41.6 | 0.5 | 41.3 | 41.3 | 41.1 | 40.8 | 0.6 | 0.7 | 1.1 | 1.9 |
| Liq. | 273.2 | 12.71 | 685.5 | 1.5 | 667.5 | 674.7 | 641.7 | 665.8 | 2.6 | 1.6 | 6.4 | 2.9 |
| Liq. | 273.2 | 20.89 | 740.2 | 1.4 | 738.5 | 753.7 | 712.7 | 723.2 | 0.2 | 1.8 | 3.7 | 2.3 |
| Liq. | 273.2 | 52.28 | 838.1 | 1.3 | 858.1 | 889.7 | 833.2 | 824.2 | 2.4 | 6.2 | 0.6 | 1.7 |
| Liq. | 273.2 | 103.76 | 920.2 | 1.3 | 947.6 | 987.6 | 918.5 | 906.3 | 3.0 | 7.3 | 0.2 | 1.5 |
| Liq. | 273.2 | 124.50 | 944.3 | 1.3 | 971.3 | 1,012.6 | 940.1 | 929.8 | 2.9 | 7.2 | 0.5 | 1.5 |
| Gas | 283.3 | 1.12 | 18.7 | 0.4 | 19.1 | 19.2 | 19.2 | 19.1 | 2.1 | 2.5 | 2.3 | 1.7 |
| Gas | 283.3 | 2.09 | 36.8 | 0.4 | 38.0 | 38.2 | 38.0 | 37.7 | 3.3 | 3.8 | 3.5 | 2.5 |
| Gas | 283.3 | 4.87 | 110.8 | 0.8 | 117.7 | 117.1 | 116.1 | 114.7 | 6.2 | 5.6 | 4.7 | 3.4 |
| Liq. | 283.3 | 9.52 | 564.7 | 2.1 | 531.5 | 529.3 | 508.8 | 544.2 | 5.9 | 6.3 | 9.9 | 3.6 |
| Liq. | 283.3 | 20.63 | 701.4 | 1.3 | 697.0 | 707.5 | 671.3 | 686.1 | 0.6 | 0.9 | 4.3 | 2.2 |
| Liq. | 283.3 | 51.89 | 814.3 | 1.3 | 834.0 | 864.0 | 810.6 | 802.2 | 2.4 | 6.1 | 0.5 | 1.5 |
| Liq. | 283.3 | 103.37 | 902.8 | 1.3 | 930.4 | 970.8 | 903.9 | 890.2 | 3.1 | 7.5 | 0.1 | 1.4 |
| Liq. | 283.3 | 125.37 | 929.6 | 1.3 | 957.1 | 999.1 | 928.5 | 916.3 | 3.0 | 7.5 | 0.1 | 1.4 |
| Gas | 298.4 | 1.10 | 18.6 | 0.3 | 17.6 | 17.7 | 17.7 | 17.6 | 5.4 | 5.0 | 5.1 | 5.8 |
| Gas | 298.4 | 2.09 | 36.0 | 0.4 | 35.2 | 35.4 | 35.3 | 35.0 | 2.3 | 1.6 | 1.8 | 2.8 |
| Gas | 298.4 | 5.18 | 108.2 | 0.6 | 108.0 | 109.9 | 108.9 | 107.2 | 0.2 | 1.5 | 0.7 | 0.9 |
| SC | 298.4 | 10.96 | 462.0 | 2.0 | 438.7 | 431.4 | 417.7 | 445.3 | 5.0 | 6.6 | 9.6 | 3.6 |
| SC | 298.3 | 20.83 | 642.9 | 1.3 | 636.7 | 640.5 | 610.7 | 631.1 | 1.0 | 0.4 | 5.0 | 1.8 |
| SC | 298.3 | 51.73 | 779.9 | 1.2 | 799.4 | 826.4 | 777.5 | 770.6 | 2.5 | 6.0 | 0.3 | 1.2 |
| SC | 298.3 | 102.11 | 873.8 | 1.2 | 904.2 | 944.7 | 881.2 | 865.8 | 3.5 | 8.1 | 0.9 | 0.9 |
| SC | 298.3 | 124.97 | 903.9 | 1.3 | 934.4 | 977.3 | 909.6 | 894.9 | 3.4 | 8.1 | 0.6 | 1.0 |
| Gas | 323.4 | 1.22 | 19.3 | 0.3 | 17.8 | 17.9 | 17.9 | 17.8 | 7.6 | 7.2 | 7.3 | 7.9 |
| Gas | 323.5 | 2.11 | 32.7 | 0.3 | 32.0 | 32.2 | 32.1 | 31.9 | 2.3 | 1.6 | 1.8 | 2.7 |
| Gas | 323.4 | 5.23 | 90.6 | 0.5 | 90.9 | 92.3 | 91.7 | 90.3 | 0.3 | 1.9 | 1.2 | 0.3 |
| SC | 323.5 | 11.81 | 316.8 | 1.1 | 308.5 | 296.1 | 289.6 | 297.6 | 2.6 | 6.5 | 8.6 | 6.1 |
| SC | 323.5 | 20.23 | 531.8 | 1.1 | 520.9 | 513.0 | 493.7 | 519.3 | 2.0 | 3.5 | 7.2 | 2.3 |
| SC | 323.4 | 49.82 | 718.0 | 1.1 | 735.2 | 755.2 | 714.1 | 712.1 | 2.4 | 5.2 | 0.5 | 0.8 |
| SC | 323.4 | 103.43 | 837.2 | 1.2 | 866.4 | 906.0 | 847.5 | 830.8 | 3.5 | 8.2 | 1.2 | 0.8 |
| SC | 323.5 | 124.84 | 868.2 | 1.2 | 898.0 | 940.9 | 878.0 | 860.7 | 3.4 | 8.4 | 1.1 | 0.9 |
| Gas | 373.5 | 2.10 | 24.5 | 0.3 | 26.6 | 26.8 | 26.7 | 26.5 | 8.8 | 9.3 | 9.0 | 8.4 |
| Gas | 373.6 | 5.24 | 68.9 | 0.3 | 71.3 | 72.0 | 71.6 | 70.9 | 3.5 | 4.5 | 3.9 | 2.9 |
| Gas | 373.6 | 10.43 | 156.3 | 0.4 | 159.4 | 160.7 | 158.7 | 158.4 | 1.9 | 2.8 | 1.5 | 1.3 |
| SC | 373.6 | 20.73 | 364.2 | 0.7 | 359.6 | 349.7 | 340.6 | 353.9 | 1.2 | 4.0 | 6.5 | 2.8 |
| SC | 373.6 | 46.52 | 601.3 | 0.9 | 608.4 | 614.1 | 586.6 | 593.9 | 1.2 | 2.1 | 2.4 | 1.2 |
| SC | 373.5 | 63.34 | 668.4 | 1.0 | 684.5 | 701.9 | 666.2 | 663.4 | 2.4 | 5.0 | 0.3 | 0.7 |
| SC | 373.5 | 63.16 | 667.7 | 1.0 | 683.8 | 701.1 | 665.5 | 662.8 | 2.4 | 5.0 | 0.3 | 0.7 |
| SC | 373.6 | 103.40 | 767.8 | 1.1 | 792.4 | 826.6 | 777.6 | 761.5 | 3.2 | 7.7 | 1.3 | 0.8 |
| SC | 373.6 | 122.28 | 800.7 | 1.1 | 826.6 | 865.5 | 812.0 | 793.3 | 3.2 | 8.1 | 1.4 | 0.9 |
| SC | 373.6 | 125.29 | 804.9 | 1.1 | 831.4 | 871.0 | 816.8 | 797.9 | 3.3 | 8.2 | 1.5 | 0.9 |
| Gas | 423.4 | 2.12 | 23.2 | 0.2 | 23.3 | 23.4 | 23.3 | 23.2 | 0.7 | 1.0 | 0.8 | 0.4 |
| Gas | 423.4 | 5.22 | 58.2 | 0.3 | 59.8 | 60.1 | 59.8 | 59.5 | 2.8 | 3.3 | 2.8 | 2.3 |
| Gas | 423.4 | 10.36 | 120.5 | 0.3 | 125.9 | 126.2 | 125.0 | 124.9 | 4.5 | 4.8 | 3.8 | 3.7 |
| Gas | 423.4 | 20.94 | 258.3 | 0.5 | 271.3 | 267.7 | 262.3 | 268.3 | 5.0 | 3.6 | 1.6 | 3.9 |
| SC | 423.5 | 29.08 | 371.6 | 0.6 | 370.1 | 363.0 | 353.3 | 364.4 | 0.4 | 2.3 | 4.9 | 2.0 |
| SC | 423.5 | 49.87 | 527.2 | 0.8 | 534.5 | 535.3 | 514.3 | 522.2 | 1.4 | 1.5 | 2.4 | 1.0 |
| SC | 423.5 | 103.36 | 704.5 | 0.9 | 725.8 | 753.1 | 712.3 | 698.8 | 3.0 | 6.9 | 1.1 | 0.8 |
| SC | 423.5 | 124.80 | 746.2 | 1.0 | 770.1 | 803.8 | 757.4 | 739.5 | 3.2 | 7.7 | 1.5 | 0.9 |
| | | | | *AAD* / % | | | | | 3.0 | 5.0 | 2.9 | 2.2 |

The standard uncertainty for the temperature, pressure and period are:
$u(T)$ = 0.02 K, $u(p)$ = 0.02 MPa and $u(\tau)$ = 0.005 μs

Table 10. Uncertainties of density measurements for each mixture with 95% level of confidence ($k$=2)

| | | | Average | | Max | |
|---|---|---|---|---|---|---|
| Material | Phase | No | $U(\rho)$/ kg.m$^{-3}$ | $U(\rho)$/% | $U(\rho)$/ kg.m$^{-3}$ | $U(\rho)$/% |
| MIX 1 | Gas | 24 | 0.94 | 1.8 | 2.64 | 4.5 |
| | Liquid | 22 | 4.01 | 0.4 | 7.28 | 0.9 |
| | SC | 17 | 3.43 | 0.4 | 7.58 | 1.2 |
| | Total | 63 | 2.68 | 1.0 | 7.58 | 4.5 |
| MIX 2 | Gas | 12 | 0.81 | 2.0 | 1.06 | 2.9 |
| | Liquid | 11 | 2.83 | 0.3 | 5.80 | 0.7 |
| | SC | 20 | 2.28 | 0.4 | 7.07 | 1.3 |
| | Total | 43 | 2.01 | 0.8 | 7.07 | 2.9 |
| MIX 3 | Gas | 18 | 0.79 | 1.9 | 1.62 | 3.9 |
| | Liquid | 10 | 2.79 | 0.4 | 4.10 | 0.7 |
| | SC | 21 | 2.16 | 0.3 | 3.92 | 0.8 |
| | Total | 49 | 1.74 | 0.9 | 4.10 | 3.9 |
| Total | Gas | 54 | 0.86 | 1.9 | 2.64 | 4.5 |
| | Liquid | 43 | 3.43 | 0.4 | 7.28 | 0.9 |
| | SC | 58 | 2.57 | 0.4 | 7.58 | 1.3 |
| | Total | **155** | **2.20** | **0.9** | **7.58** | **4.5** |

Table 11. AAD and Max. Deviations of this work using PR, SRK and GERG EoSs

| Mixture | Phase | No | *AAD* / % | | | | | | | *MAD* / % | | | | | | |
|---|---|---|---|---|---|---|---|---|---|---|---|---|---|---|---|---|
| | | | PR-$CO_2$ | SRK-$CO_2$ | PR | SRK | PR-Pen | SRK-Pen | GERG | PR-$CO_2$ | SRK-$CO_2$ | PR | SRK | PR-Pen | SRK-Pen | GERG |
| MIX 1 | Gas | 24 | 3.1 | 3.2 | 3.8 | 2.8 | 3.5 | 3.0 | 2.6 | 7.7 | 7.6 | 8.4 | 10.2 | 8.3 | 7.7 | 6.1 |
| | Liquid | 22 | 1.5 | 1.2 | 5.9 | 5.4 | 2.7 | 4.6 | 0.8 | 2.1 | 1.9 | 8.7 | 13.8 | 7.2 | 9.3 | 2.4 |
| | SC | 17 | 1.4 | 0.7 | 5.3 | 5.0 | 2.8 | 4.8 | 0.8 | 1.7 | 1.2 | 8.7 | 12.0 | 6.5 | 7.9 | 1.4 |
| | Total | 63 | 2.1 | 1.8 | 4.9 | 4.3 | 3.0 | 4.1 | 1.5 | 7.7 | 7.6 | 8.7 | 13.8 | 8.3 | 9.3 | 6.1 |
| MIX 2 | Gas | 12 | 2.4 | 2.3 | 2.4 | 2.5 | 2.3 | 2.4 | 2.4 | 8.1 | 7.8 | 8.8 | 7.5 | 8.4 | 7.8 | 7.9 |
| | Liquid | 11 | 1.4 | 1.2 | 5.2 | 5.9 | 2.5 | 4.4 | 0.5 | 2.5 | 3.3 | 8.7 | 12.0 | 6.3 | 7.4 | 1.3 |
| | SC | 20 | 1.2 | 1.3 | 5.1 | 6.6 | 3.5 | 5.4 | 1.3 | 3.5 | 4.4 | 7.7 | 12.4 | 8.1 | 9.4 | 5.3 |
| | Total | 43 | 1.6 | 1.6 | 4.3 | 5.3 | 2.9 | 4.3 | 1.4 | 8.1 | 7.8 | 8.8 | 12.4 | 8.4 | 9.4 | 7.9 |
| MIX 3 | Gas | 18 | 3.5 | 3.0 | 3.6 | 2.9 | 3.2 | 2.8 | 3.2 | 8.8 | 8.2 | 9.3 | 8.0 | 9.0 | 8.2 | 8.4 |
| | Liquid | 10 | 2.6 | 2.8 | 5.2 | 6.4 | 2.6 | 4.3 | 2.0 | 5.9 | 8.7 | 7.5 | 14.0 | 9.9 | 10.8 | 3.6 |
| | SC | 21 | 2.6 | 1.9 | 5.7 | 5.5 | 2.8 | 4.7 | 1.5 | 5.0 | 7.2 | 8.4 | 13.0 | 9.6 | 10.3 | 6.1 |
| | Total | 49 | 3.0 | 2.4 | 5.0 | 4.6 | 2.9 | 3.9 | 2.2 | 8.8 | 8.7 | 9.3 | 14.0 | 9.9 | 10.8 | 8.4 |
| Total | Gas | 54 | 3.1 | 2.9 | 3.4 | 2.8 | 3.2 | 2.8 | 2.8 | 8.8 | 8.2 | 9.3 | 10.2 | 9.0 | 8.2 | 8.4 |
| | Liquid | 43 | 1.7 | 1.6 | 5.5 | 5.8 | 2.6 | 4.5 | 1.0 | 5.9 | 8.7 | 8.7 | 14.0 | 9.9 | 10.8 | 3.6 |
| | SC | 58 | 1.7 | 1.3 | 5.4 | 5.7 | 3.1 | 5.0 | 1.2 | 5.0 | 7.2 | 8.7 | 13.0 | 9.6 | 10.3 | 6.1 |
| | Total | 155 | 2.2 | 1.9 | 4.8 | 4.7 | 3.0 | 4.1 | 1.7 | 8.8 | 8.7 | 9.3 | 14.0 | 9.9 | 10.8 | 8.4 |

Table 12. Density reduction of pure $CO_2$ at supercritical area at the temperature of 323.15 K

| Material | *Min* / % | *p* / MPa |
|---|---|---|
| MIX 1 | -20.1 | 11.01 |
| MIX 2 | -33.9 | 11.01 |
| MIX 3 | -45.9 | 12.39 |

Table 13. AADs of the calculated thermodynamic properties from the GERG EoS

| Mixture | Phase | No | *AAD* / % | | | | |
|---|---|---|---|---|---|---|---|
| | | | $\rho$ | *Z* | *Cp* | *SoS* | $\mu_{JT}$ |
| MIX 1 | Gas | 24 | 3.0 | 2.9 | 1.2 | 0.9 | 4.0 |
| | Liquid | 22 | 0.8 | 0.8 | 0.6 | 4.4 | 3.1 |
| | SC | 17 | 0.8 | 0.8 | 0.7 | 1.0 | 4.8 |
| | Total | 63 | 1.6 | 1.6 | 0.8 | 2.1 | 3.9 |
| MIX 2 | Gas | 12 | 2.5 | 2.4 | 4.1 | 0.3 | 12.3 |
| | Liquid | 11 | 0.5 | 0.5 | 7.5 | 15.1 | 26.5 |
| | SC | 20 | 1.3 | 1.4 | 9.6 | 5.6 | 11.5 |
| | Total | 43 | 1.4 | 1.4 | 7.5 | 6.6 | 15.6 |
| MIX 3 | Gas | 18 | 3.2 | 3.2 | 1.9 | 0.2 | 2.0 |
| | Liquid | 10 | 2.0 | 2.1 | 5.2 | 3.1 | 8.3 |
| | SC | 21 | 1.5 | 1.6 | 4.0 | 1.1 | 12.7 |
| | Total | 49 | 2.3 | 2.2 | 3.5 | 1.1 | 7.9 |
| Total | Gas | 54 | 2.9 | 2.9 | 2.1 | 0.5 | 5.2 |
| | Liquid | 43 | 1.0 | 1.0 | 3.4 | 6.8 | 10.3 |
| | SC | 58 | 1.2 | 1.3 | 5.0 | 2.6 | 10.0 |
| | Total | 155 | 1.8 | 1.7 | 3.5 | 3.1 | 8.4 |

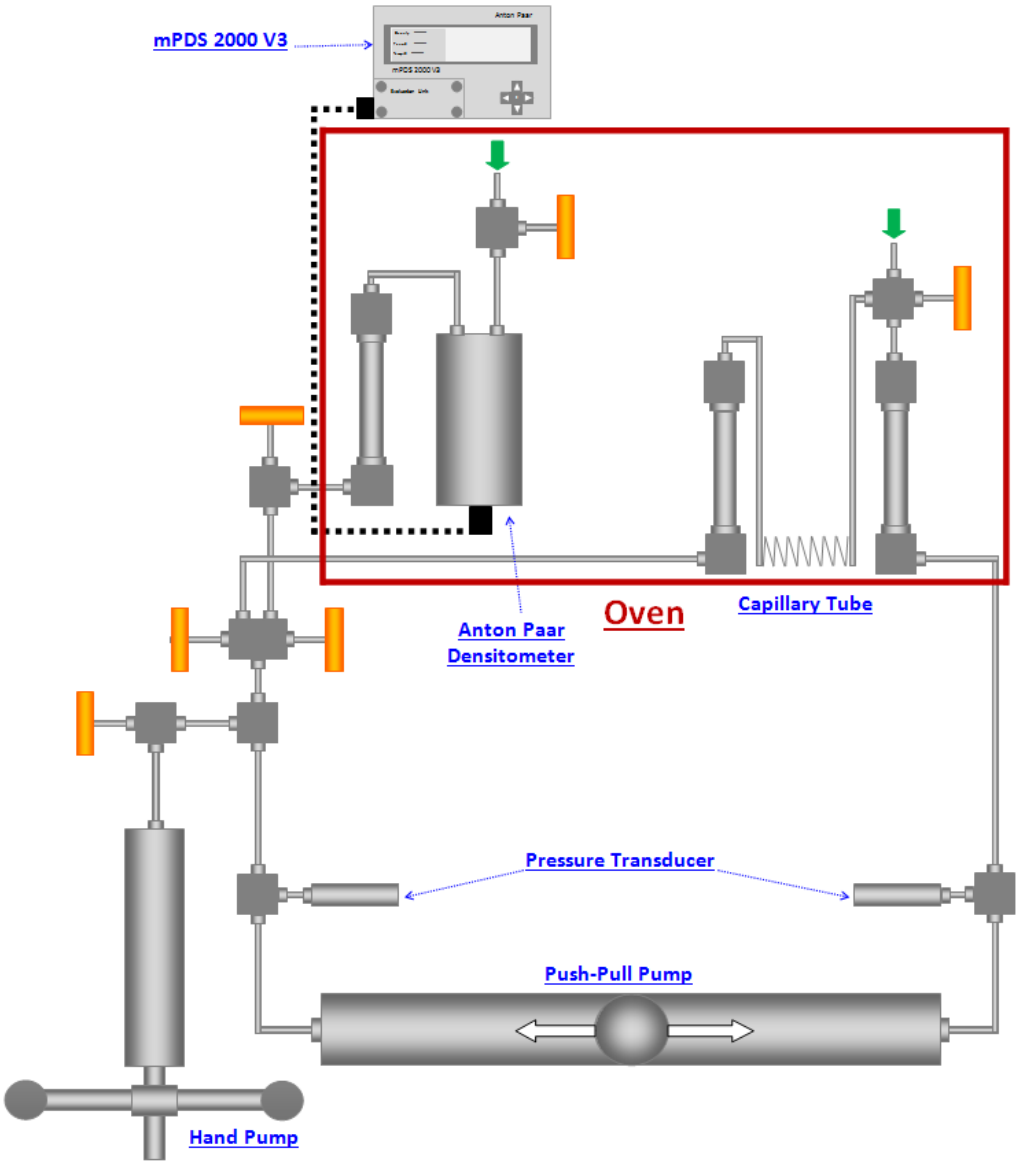


Figure 1. A schematic view of the viscosity experimental setup

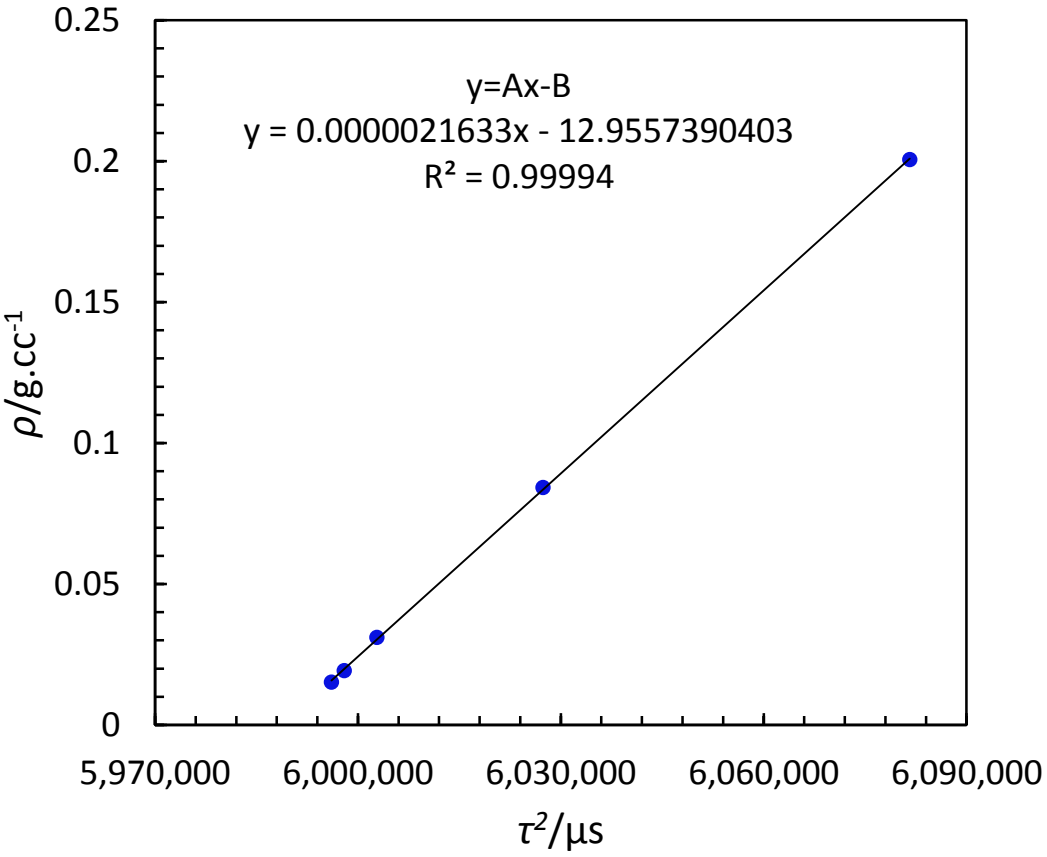


Figure 2. Calibration procedure using pure $CO_2$ at 373.15 K at low pressures (gas phase)

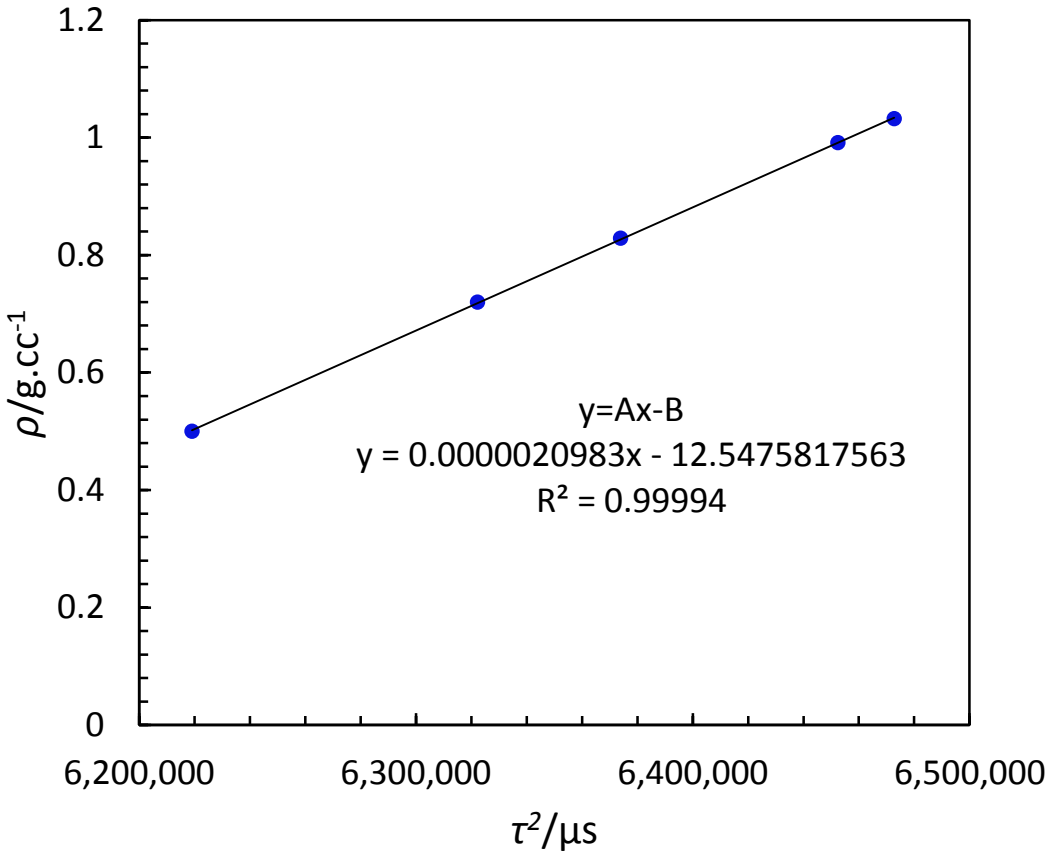


Figure 3. Calibration procedure using pure $CO_2$ at 373.15 K at high pressures (dense phase)

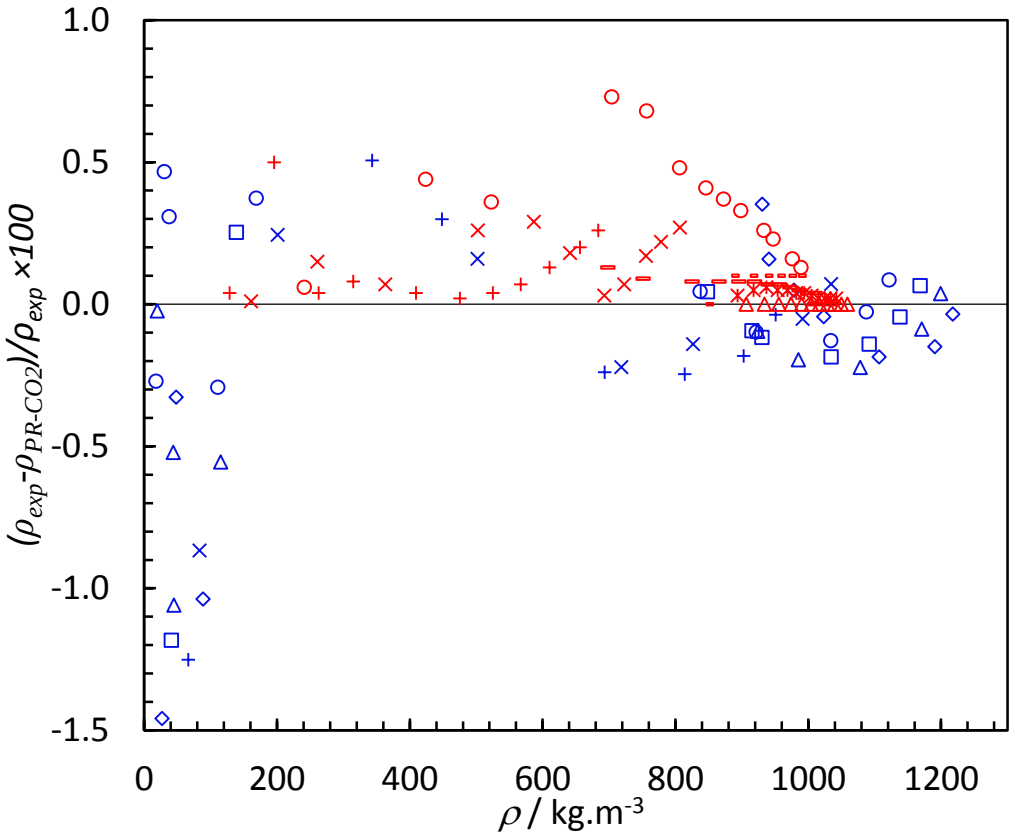


Figure 4. Validation data of pure $CO_2$ density at different isotherms

This work: (◊): 273.2 K, (Δ): 283.2 K, (□): 298.2 K, (○): 323.2 K, (×): 373.2 K, (+): 423.2 K
Al-Siyabi et al. [41]: (Δ): 283.2 K, (): 288.2 K, (-): 293.2 K, (_): 301.2 K, (○): 323.15 K, (×): 373.15 K, (+): 423.15 K

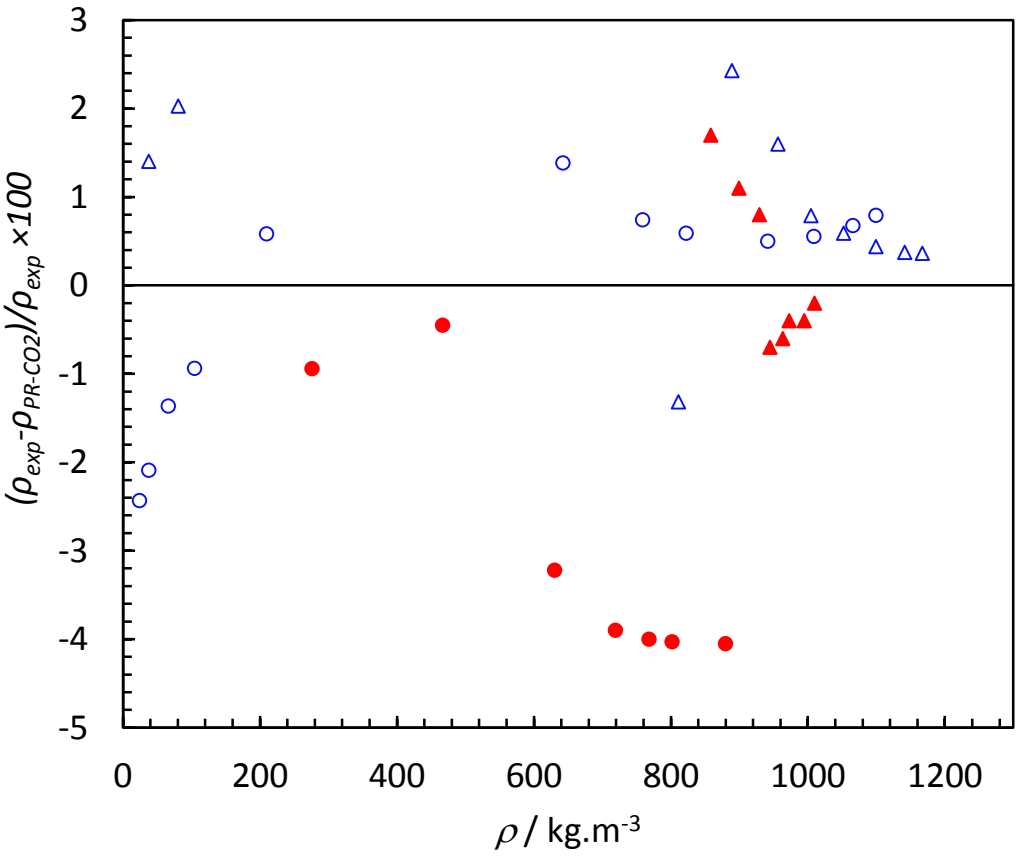


Figure 5. Density validation data at two isotherms for MIX 1

This work: (Δ): 283.2 K, (○): 323.2 K, Al-Siyabi et al. [41]:(▲): 283.2 K, (●): 323.2 K

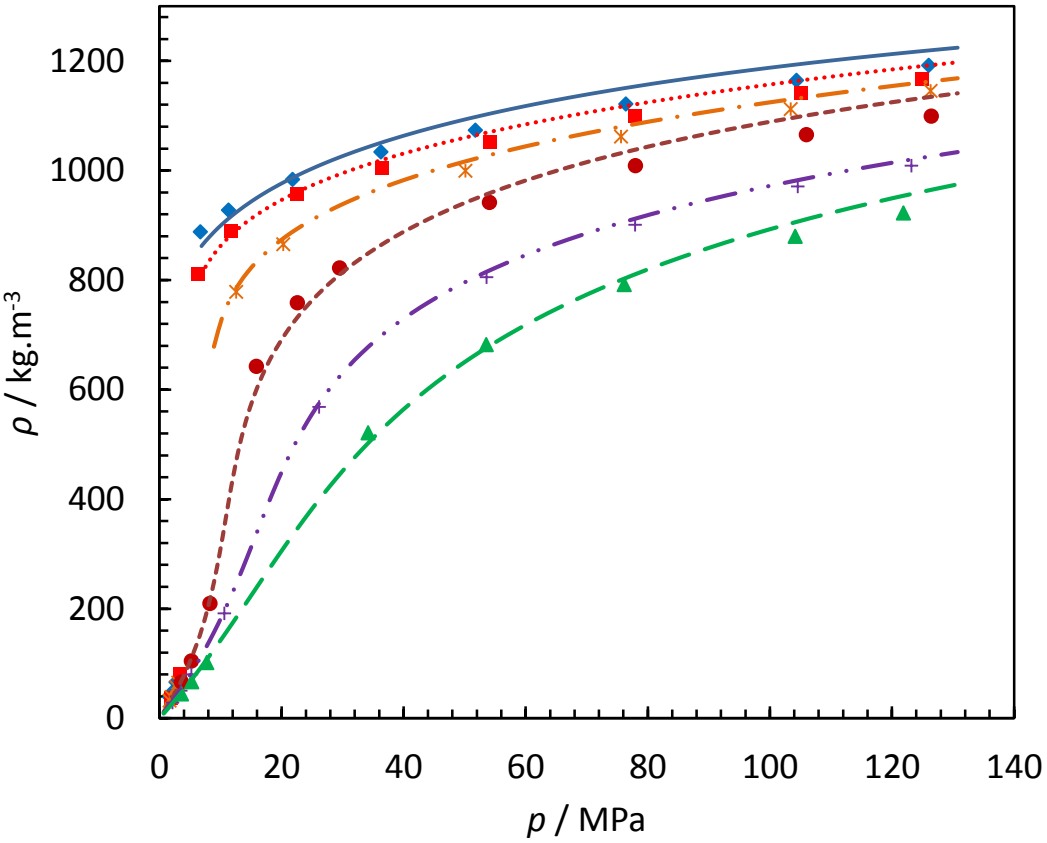


Figure 6. Experimental and modeling results of MIX 1
Experimental / modeling (PR-$CO_2$) results: (♦/—) at 273.15 K, (■/….) at 283.15 K, (x/—.) at 298.15 K, (●/----) at 323.15 K, (+/—..) at 373.15 K and (▲/— —) at 423.15 K

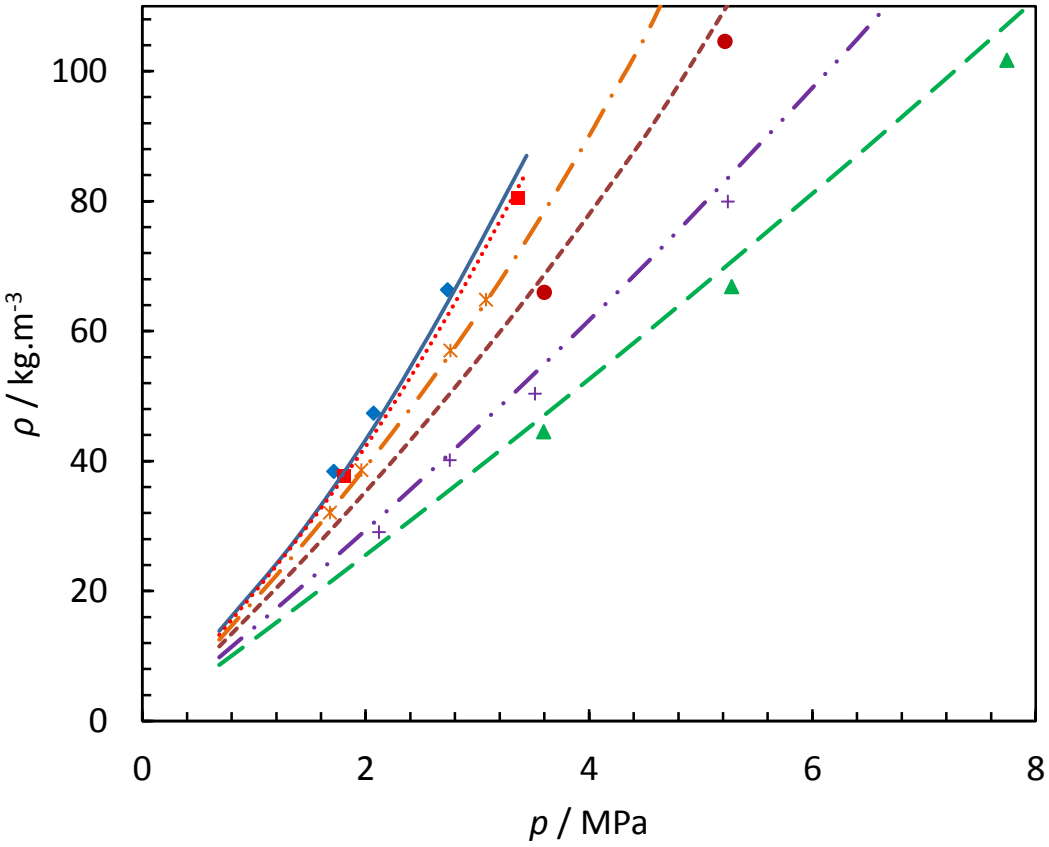


Figure 7. Experimental and modeling results of MIX 1 at lower pressures
Experimental / modeling (PR-$CO_2$) results: (♦/—) at 273.15 K, (■/….) at 283.15 K, (x/—.) at 298.15 K, (●/----) at 323.15 K, (+/—..) at 373.15 K and (▲/— —) at 423.15 K

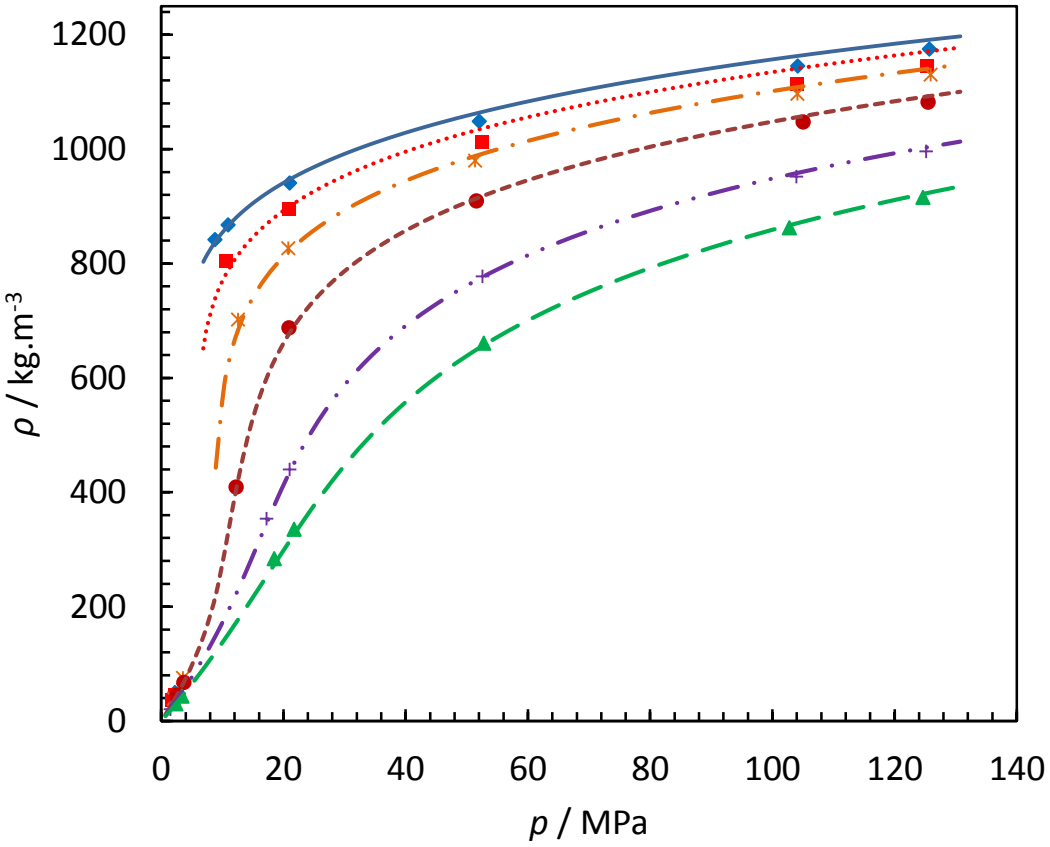


Figure 8. Experimental and modeling results of MIX 2
Experimental / modeling (PR-$CO_2$) results: (♦/—) at 273.15 K, (■/….) at 283.15 K, (x/—.) at 298.15 K, (●/----) at 323.15 K, (+/—..) at 373.15 K and (▲/— —) at 423.15 K

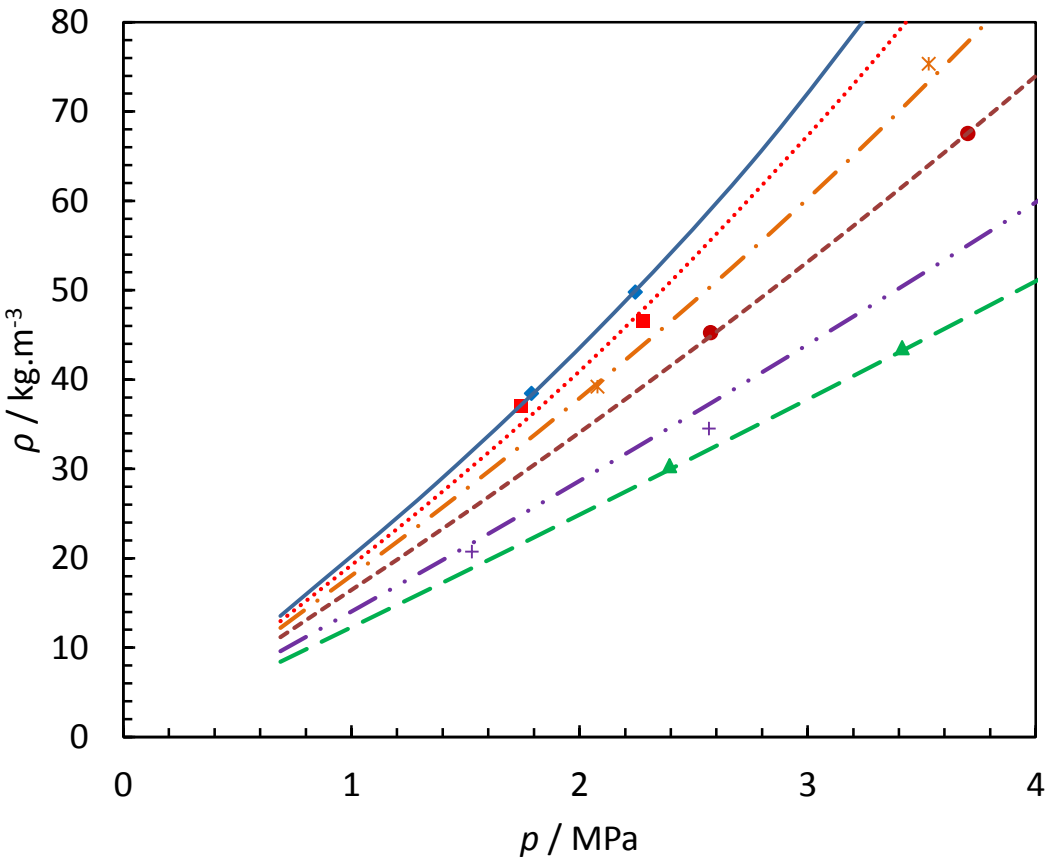


Figure 9. Experimental and modeling results of MIX 2 at low pressures
Experimental / modeling (PR-$CO_2$) results: (♦/—) at 273.15 K, (■/….) at 283.15 K, (x/—.) at 298.15 K, (●/----) at 323.15 K, (+/—..) at 373.15 K and (▲/— —) at 423.15 K

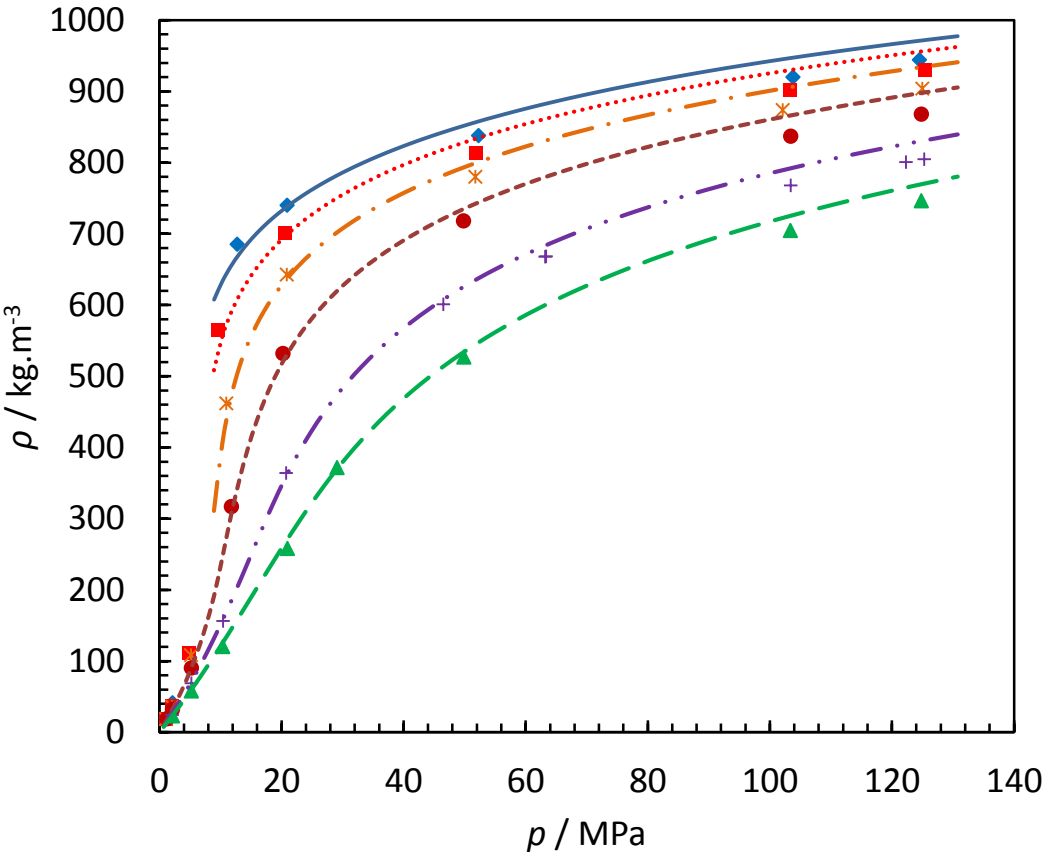


Figure 10. Experimental and modeling results of MIX 3
Experimental / modeling (PR-$CO_2$) results: (♦/—) at 273.15 K, (■/….) at 283.15 K, (x/—.) at 298.15 K, (●/----) at 323.15 K, (+/—..) at 373.15 K and (▲/— —) at 423.15 K

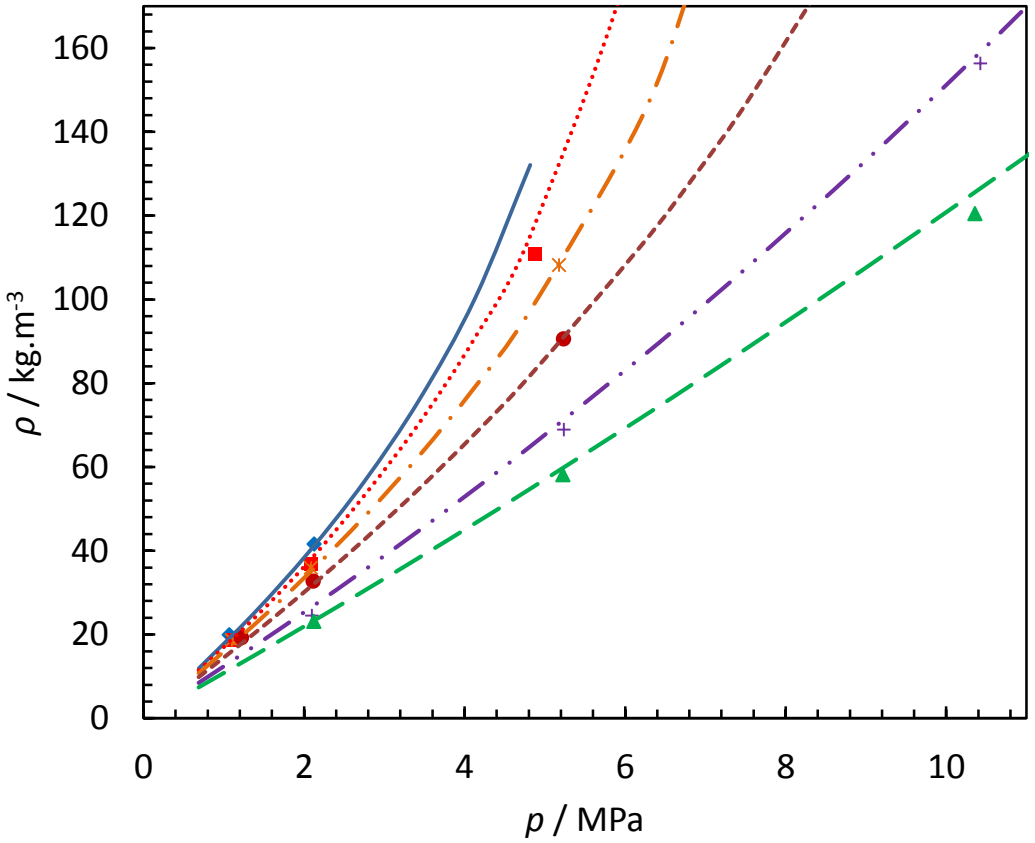


Figure 11. Experimental and modeling results of MIX 3 at low pressures
Experimental / modeling (PR-$CO_2$) results: (♦/—) at 273.15 K, (■/….) at 283.15 K, (x/—.) at 298.15 K, (●/----) at 323.15 K, (+/—..) at 373.15 K and (▲/— —) at 423.15 K

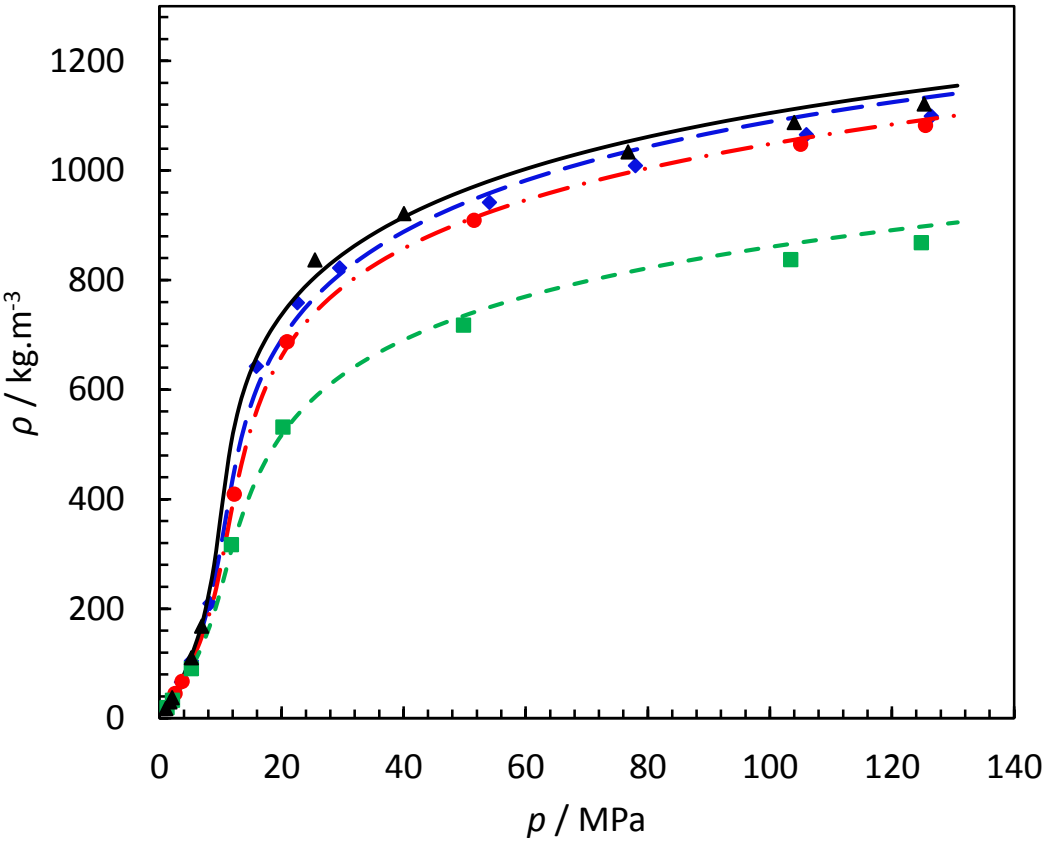


Figure 12. Effect of impurities on the density of pure $CO_2$ at supercritical area at the temperature of 323.15 K

Pure $CO_2$: (▲/___), MIX 1: (♦/_ _ _), MIX 2: (●/_._) and MIX 3: (■/----)

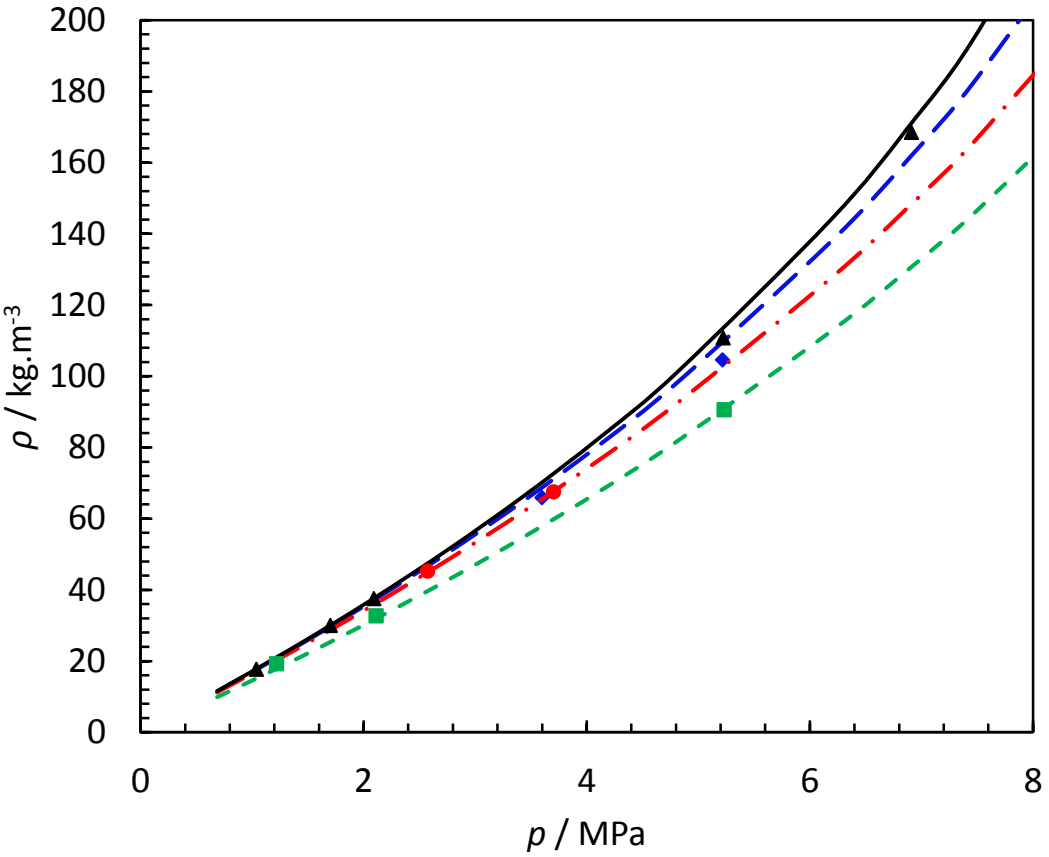


Figure 13. Effect of impurities on the density of pure $CO_2$ at supercritical area at the temperature of 323.15 K at low pressures

Pure $CO_2$: (▲/—), MIX 1: (♦/— —), MIX 2: (●/—.) and MIX 3: (■/----)

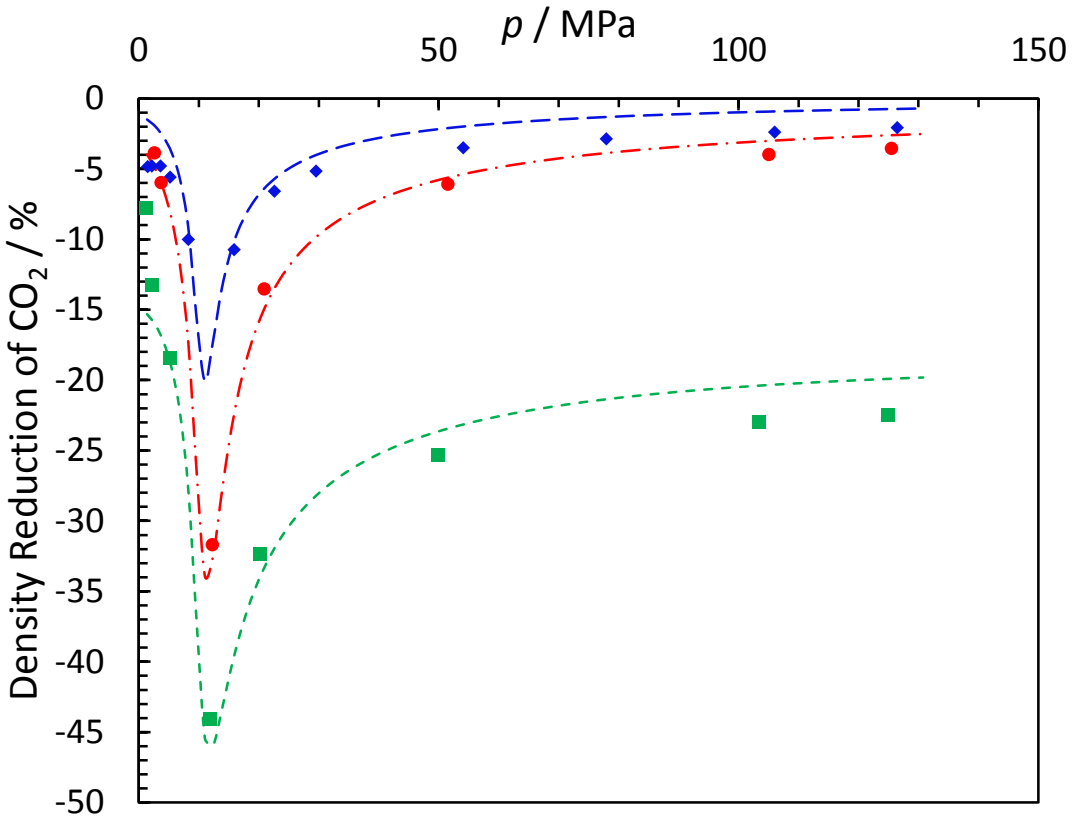


Figure 14. Density reduction of pure $CO_2$ at supercritical area, temperature 323.15 K (50 °C) MIX 1: (♦/_ _ _), MIX 2: (●/_ . _) and MIX 3: (■/----)

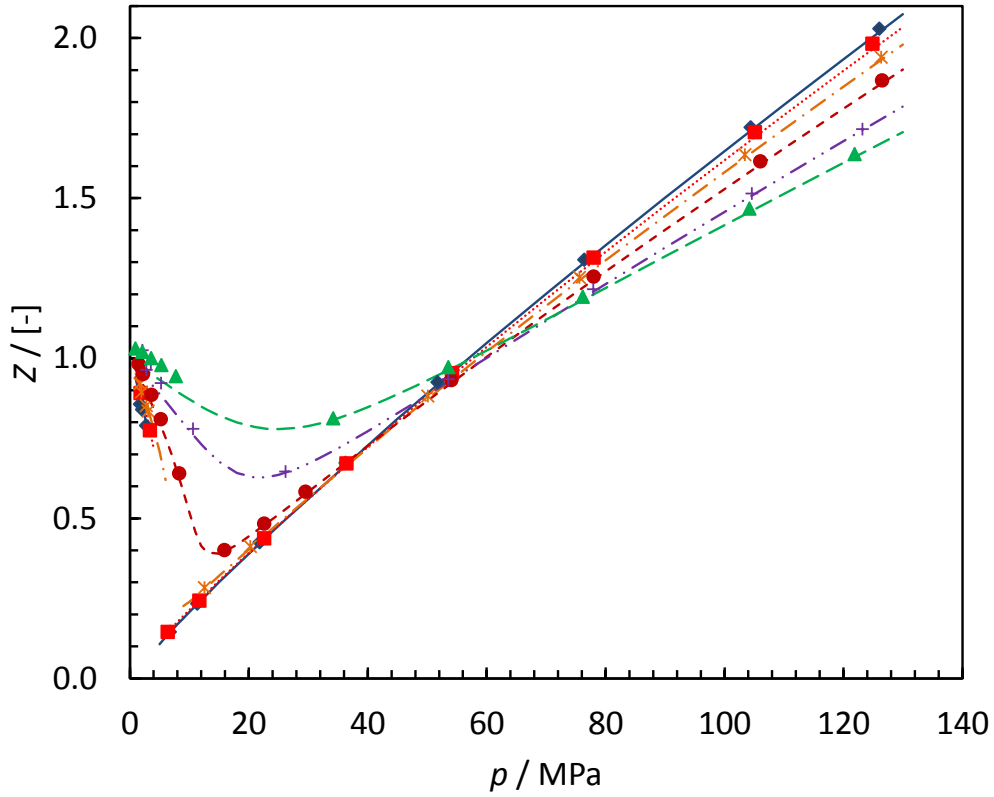


Figure 15. Compressibility factor for MIX 1 at different pressure ranges
Experimental / modeling (GERG) results: (♦/—) at 273.15 K, (■/….) at 283.15 K, (x/—.) at 298.15 K, (●/----) at 323.15 K, (+/—..) at 373.15 K and (▲/— —) at 423.15 K

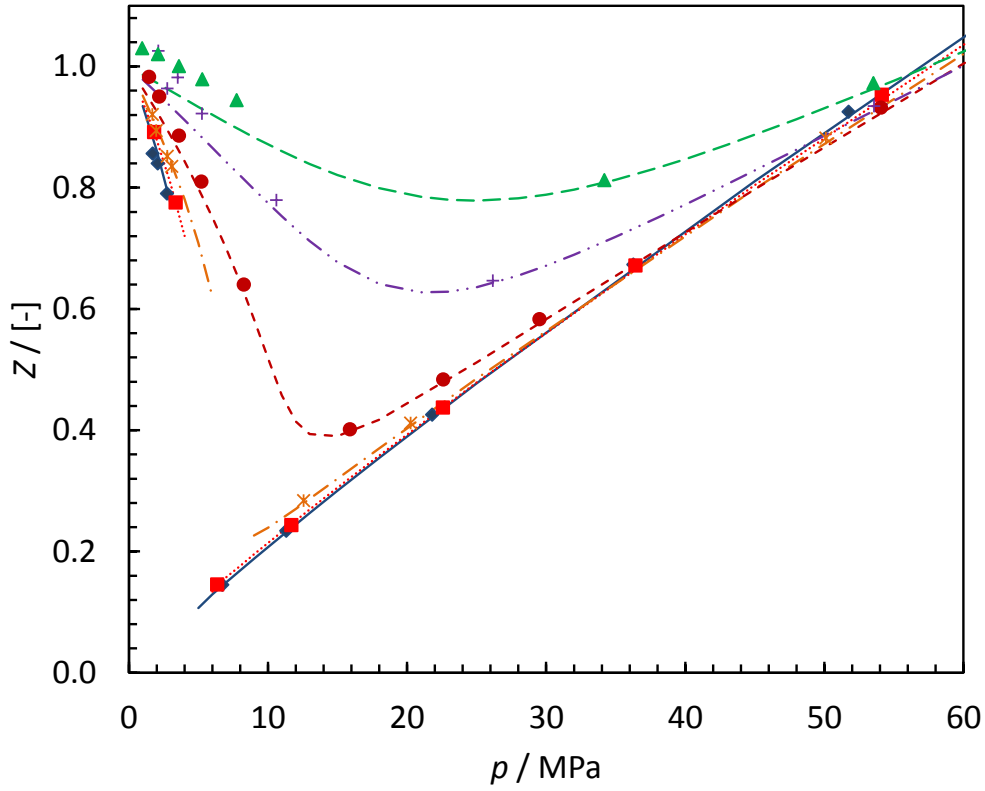


Figure 16. Compressibility factor for MIX 1 at lower pressure ranges
Experimental / modeling (GERG) results: (♦/—) at 273.15 K, (■/….) at 283.15 K, (x/—.) at 298.15 K, (●/----) at 323.15 K, (+/—..) at 373.15 K and (▲/— —) at 423.15 K

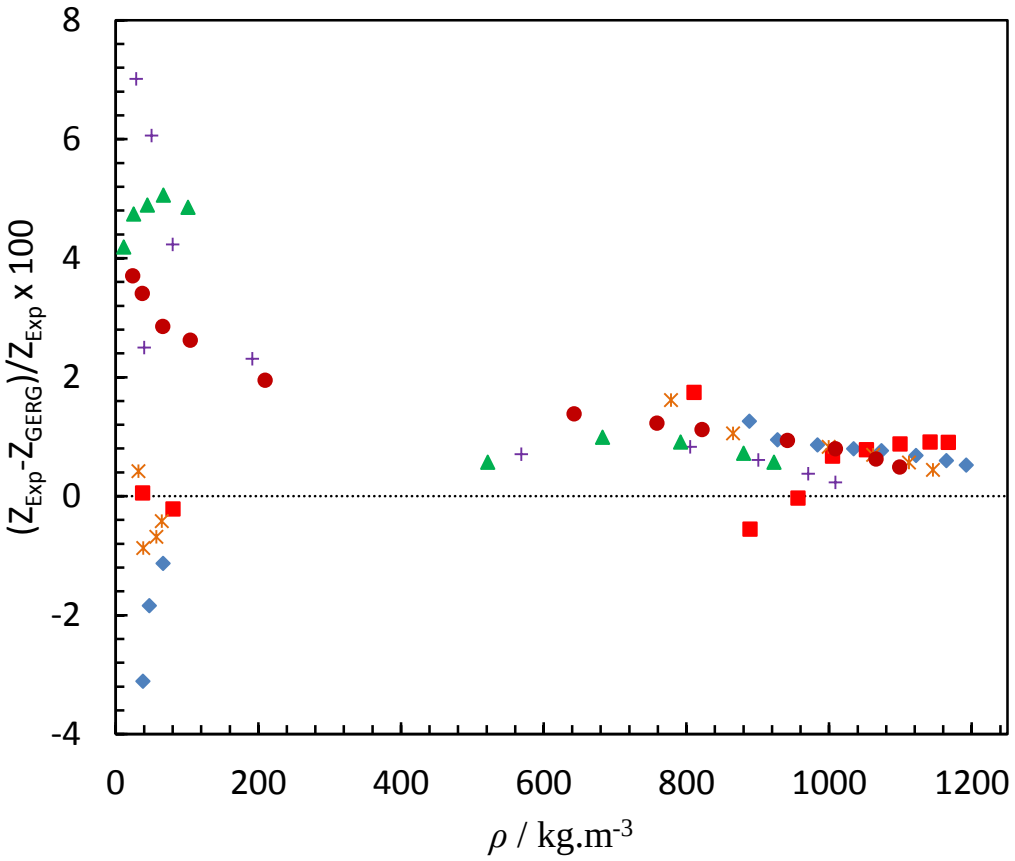


Figure 17. Deviation of compressibility factors (Z) from GERG EoS for MIX 1 at different isotherms, (♦) at 273.15 K, (■) at 283.15 K, (x) at 298.15 K, (●) at 323.15 K, (+) at 373.15 K and (▲) at 423.15 K

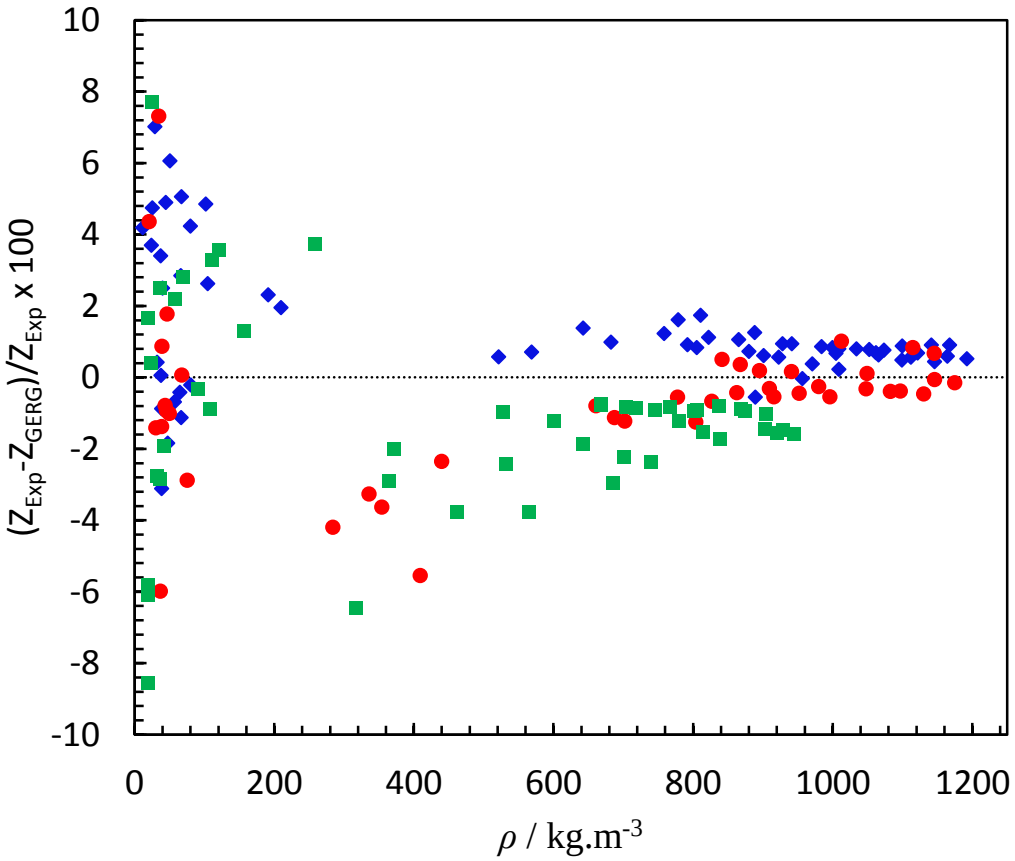


Figure 18. Deviation of compressibility factors (Z) from GERG EoS for investigated mixtures, MIX 1: (♦), MIX 2: (●) and MIX 3: (■)

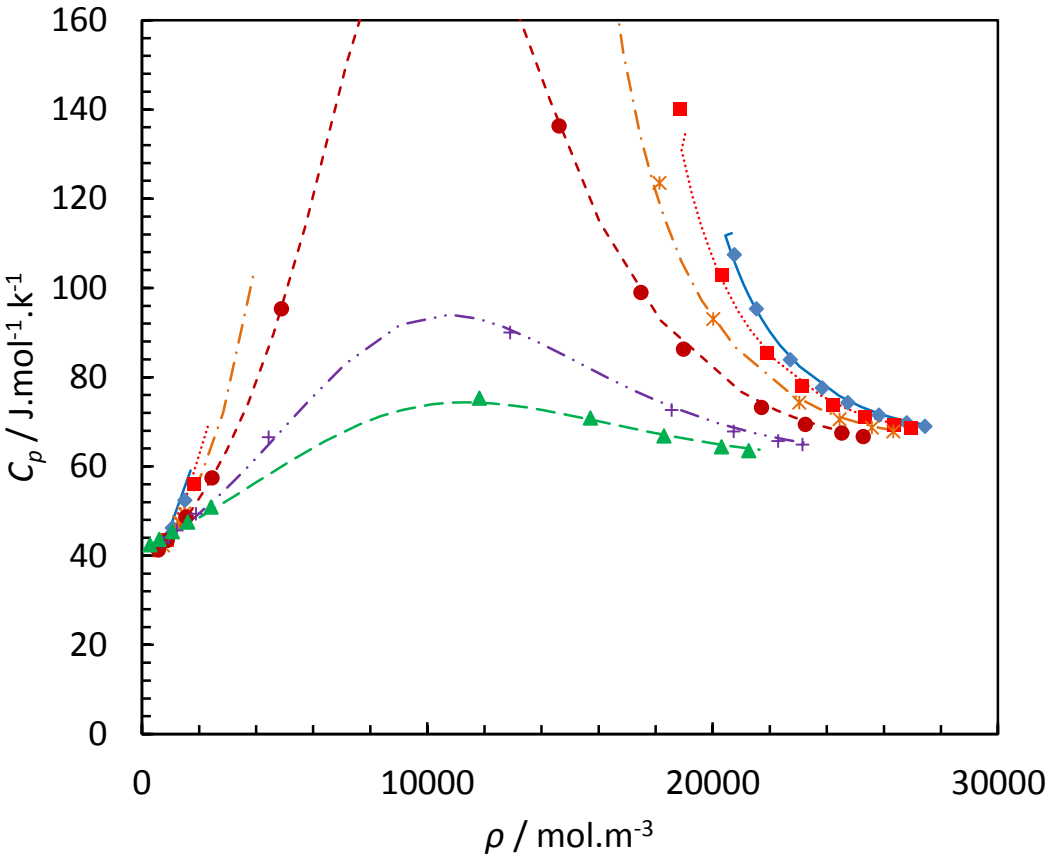


Figure 19. Specific heat capacity ($C_p$) of MIX 1 at different isotherms
Experimental / modeling (GERG) results: (♦/—) at 273.15 K, (■/….) at 283.15 K, (x/—.) at 298.15 K, (●/----) at 323.15 K, (+/—..) at 373.15 K and (▲/— —) at 423.15 K

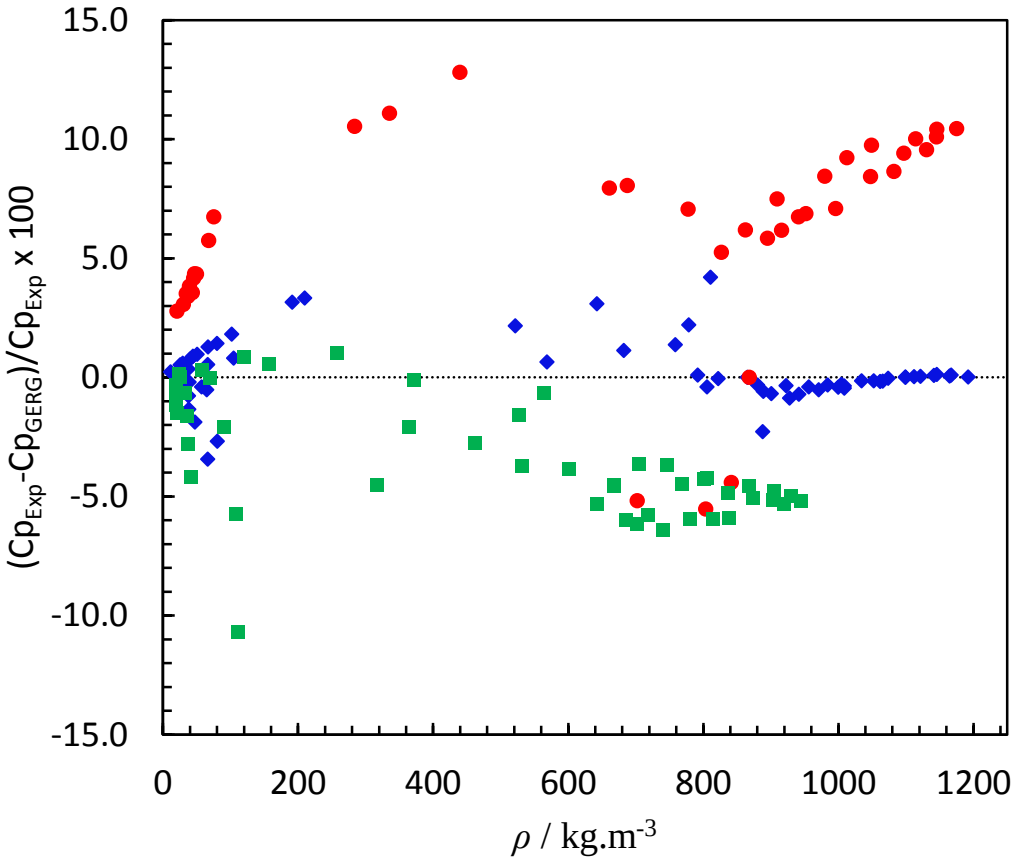


Figure 20. Deviation of specific heat capacity (Cp) from GERG EoS for investigated mixtures, MIX 1: (♦), MIX 2: (●) and MIX 3: (■)

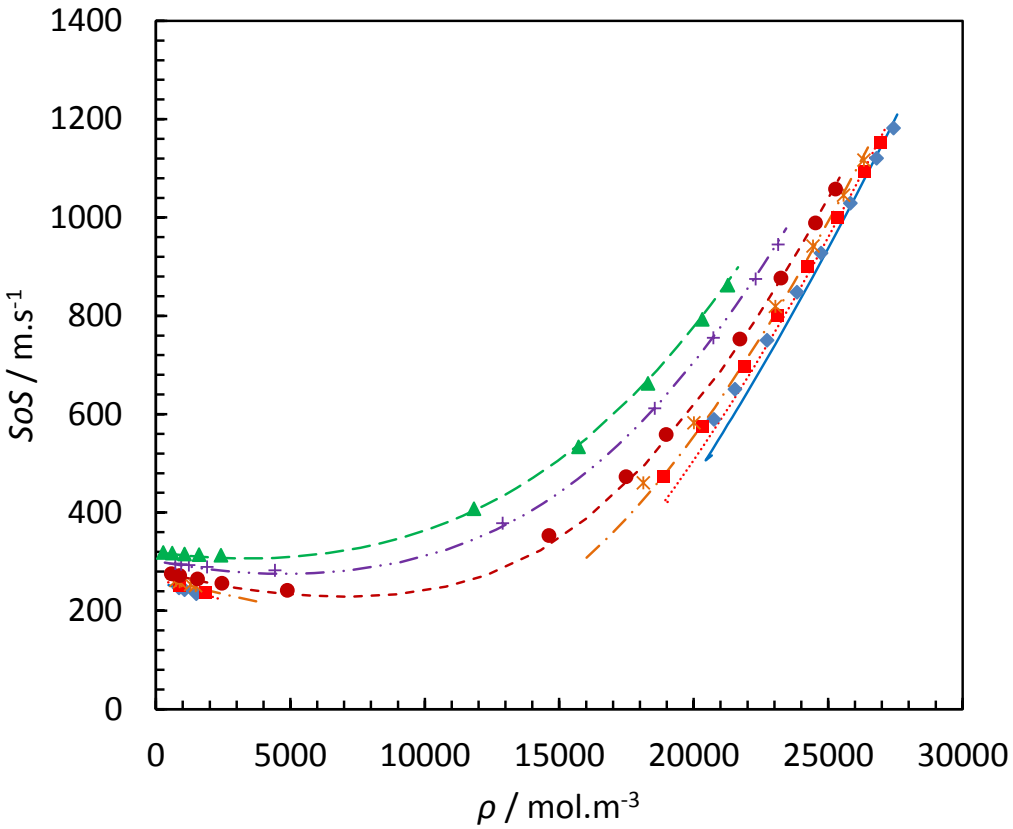


Figure 21. Speed of sound (SoS) of MIX 1 at different isotherms
Experimental / modeling (GERG) results: (♦/___) at 273.15 K, (■/….) at 283.15 K, (x/___.) at 298.15 K, (●/----) at 323.15 K, (+/___..) at 373.15 K and (▲/___ ___) at 423.15 K

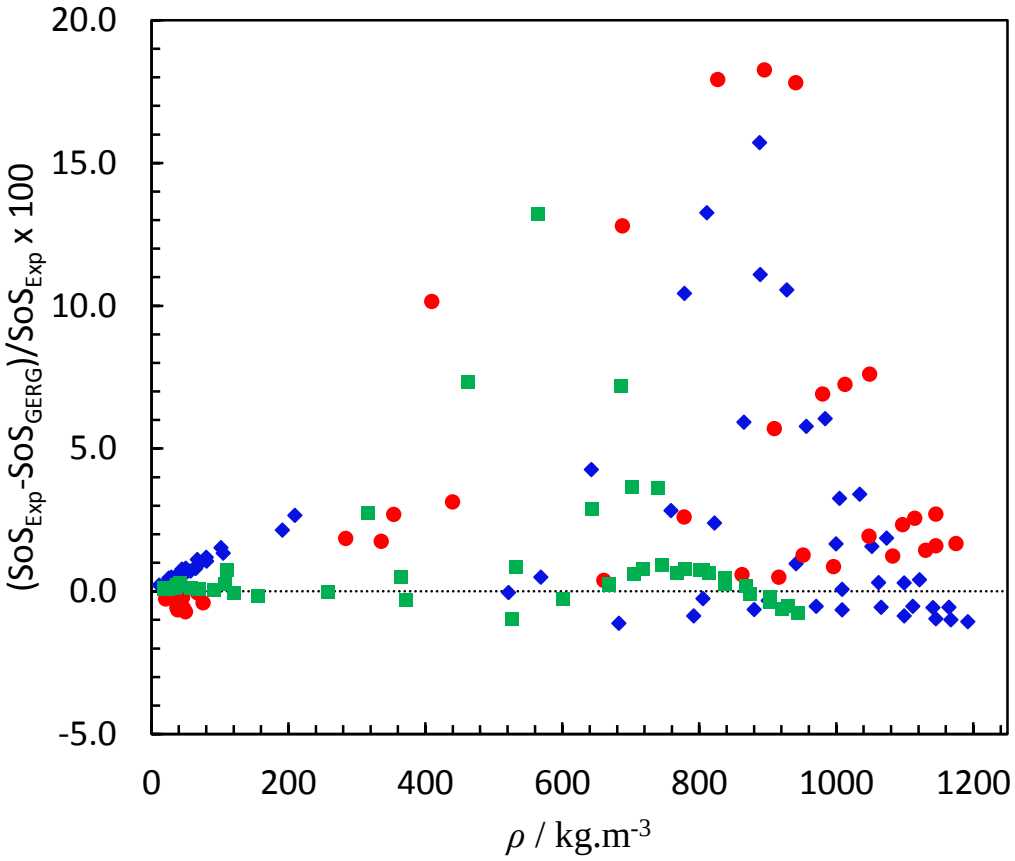


Figure 22. Deviation of speed of sound (SoS) from GERG EoS for investigated mixtures MIX 1: (♦), MIX 2: (●) and MIX 3: (■)

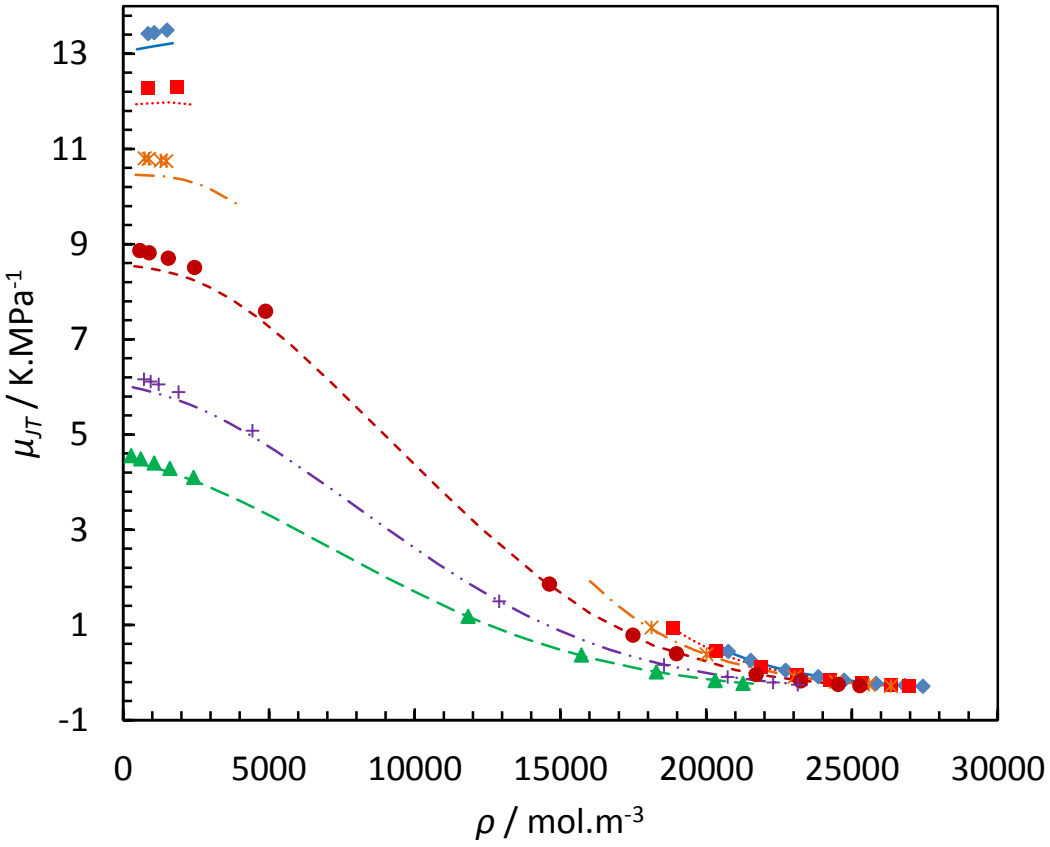


Figure 23. Joule-Thomson Coefficient ($\mu_{JT}$) of MIX 1 at different isotherms Experimental / modeling (GERG) results: (♦/___) at 273.15 K, (■/….) at 283.15 K, (x/__.) at 298.15 K, (●/----) at 323.15 K, (+/__..) at 373.15 K and (▲/__ __) at 423.15 K

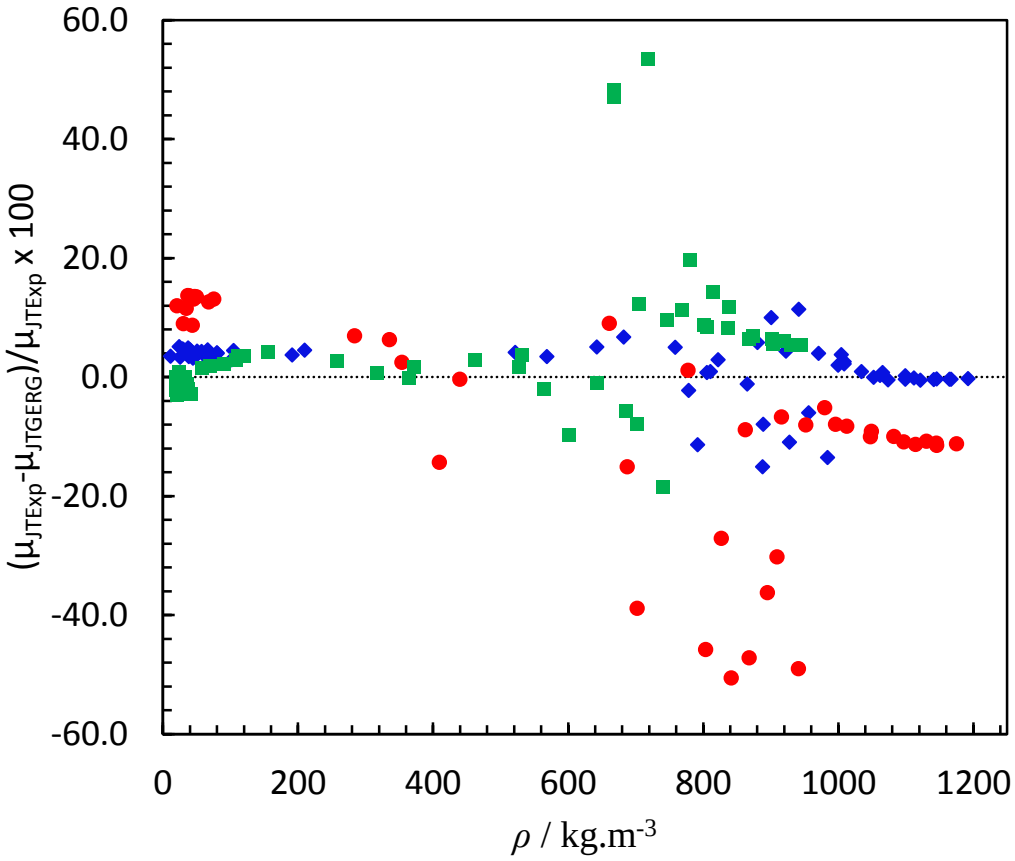


Figure 24. Deviation of Joule-Thomson Coefficient ($\mu_{JT}$) from GERG EoS for investigated mixtures, MIX 1: (♦), MIX 2: (●) and MIX 3: (■)